Protist, Vol. 170, 209–232, April 2019
http://www.elsevier.de/protis
Published online date 26 March 2019

Protist

ORIGINAL PAPER

Genomics, Biology and Phylogeny *Aurantiochytrium acetophilum* sp. nov. (Thraustrochytriaceae), Including First Evidence of Sexual Reproduction

Eneko Ganuza[a,1], Shanshan Yang[b], Magdalena Amezquita[a], Ana Giraldo-Silva[c], and Robert A. Andersen[d]

[a]Heliae Development LLC, Gilbert, AZ, USA
[b]Bioinformatics Core, The Biodesign Institute, Arizona State University, AZ, USA
[c]Center for Fundamental and Applied Microbiomics, The Biodesign Institute, Arizona State University, Tempe, AZ, USA
[d]Friday Harbor Laboratories, University of Washington, Friday Harbor, WA, USA

Submitted December 3, 2018; Accepted February 26, 2019
Monitoring Editor: David Moreira

Strain HS-399 was isolated from a mangrove swamp in Biscayne Bay (Florida, USA) and selected for its capacity to accumulate lipids (84.0 ± 1.0% DW), particularly docosahexaenoic acid (DHA; 22:6 n-3) (28.3 ± 0.1% DW). Molecular phylogenetic analysis demonstrated that the new organism belonged to the genus *Aurantiochytrium*, and when the whole nuclear genome was blasted against the type species (and only described species), *A. limacinum* SR21, there was a 5.38% difference at the protein level. We described our new organism as *Aurantiochytrium acetophilum* sp. nov. (Thraustochytriaceae, Thraustochytriales) using light microscopy, electron microscopy, substrate assimilation, biochemical composition and nuclear genomic data. We found some characteristics of biotechnological relevance that were not previously described in this family. First, strain HS-399 of *A. acetophilum* was extremely tolerant to acetate toxicity, and it used this substrate as a sole carbon source. Second, we observed putative gametes that fused together to form a zygote. Zygote fate and the life stage with meiosis were not determined; however, we found several meiosis genes in the genome, further supporting the possibility of breeding for these industrially relevant organisms.

Key words: *Aurantiochytrium*; genome; labyrinthuloid; sexual reproduction; stramenopiles; thraustochytrid.

[1]Corresponding author; fax +1 480 4242882
e-mail eganuza@heliae.com (E. Ganuza).

https://doi.org/10.1016/j.protis.2019.02.004

Introduction

Thraustochytrids were first classified as Phycomycetes or algal fungi (Sparrow 1936, 1960, 1976), but more recently they have been placed in the stramenopiles or heterokonts (Leipe et al. 1994). Organisms in the Labyrinthulales and Thraustochytriales date from the description of *Labyrinthula* (Cienkowski 1867). The Thraustochytriales currently includes 10 genera, and these are reviewed elsewhere (Andersen and Ganuza 2018; Dellero et al. 2018; Marchan et al. 2017). Genera were originally defined based upon morphology, especially the structure of the sporangium (Dick 2001), but recently morphology has been largely replaced by molecular phylogenetic analyses (e.g. Pan et al. 2017). The names for a number of taxa were not validly published because a nomenclatural type was not designated (Andersen and Ganuza 2018; Dick 2001). Ecologically, nearly all species are found in marine habitats, on decaying algal/plant matter or in coastal waters or muds (Marchan et al. 2017). Commercially, thraustochytrids are used to produce valuable lipids such us polyunsaturated fatty acids and squalene that are used for human products and animal feeds (Barclay et al. 2005; Ganuza and Izquierdo 2007; Nakazawa et al. 2012). Thraustochytrids accumulate lipids faster than any other oleaginous microorganisms (Ratledge 2013), which has brought considerable interest from the biotechnology industry. Currently, there is enough fermentation capacity projected for these organisms to support the replacement at least 15% of the global fish oil production (Craze 2018). Consequently, thraustochytrids have the biotechnological potential to yield a lasting positive environmental impact in the fisheries and aquaculture sector.

Despite the biotechnological and environmental relevance of thraustochytrids, their cell biology is understudied. For example, at least 50 production candidate-strains of *Aurantiochytrium* are reported in the literature, and yet only one species has been described and characterized with molecular phylogenetic techniques. Recently, we discovered an undescribed thraustochytrid species that was found on decaying mangrove leaves in Florida, USA and scaled its growth to commercial production level. In this paper, we describe this *Aurantiochytrium acetophilum* sp. nov. using light and electron microscopy as well as physiological, biochemical and molecular phylogenetic and genomic analyses. We report a complex pattern of life stages for this new species, and we sequence the complete nuclear and mitochondrial genomes. We provide evidence of sexual reproduction in this thraustochytrid, i.e. small spherical flagellate cells fusing to form a zygote and meiosis genes in the nuclear genome.

Results

Aurantiochytrium acetophilum E.Ganuza & R.A.Andersen sp. nov.

Diagnosis: spherical cells 3–20 μm, with relatively clear cytoplasm in log growth phase or filled with lipid vesicles in stationary phase; vegetative cell reproduction by cell division, frequently forming a tetrad of daughter cells; swimming cells formed in two sporangial types; zoospores with two laterally inserted flagella, the anteriorly directed flagellum with sinusoidal beat and the posteriorly directed flagellum with stiff sculling motion; amoebae forming directly from sporogenous cells or forming from amoebosporangia; amoebae pseudopods lobose, usually one or two lobes per cell; cysts produced; DNA sequences from genome unique and distinctive.

Holotype here designated: No. 02335123; consisting of cells from culture strain HS-399 fixed and embedded in a transmission electron microscopy block PO_4-2 deposited in the New York Botanical Garden herbarium (NY), New York City, NY USA. Name registrations: 101016 (PhycoBank) and IF556321 (Index Fungorum).

Isotype here designated: No. 02335124; consisting of cells from culture strain HS-399 fixed and embedded in a transmission electron microscopy block Caco-3 deposited in the New York Botanical Garden herbarium (NY), New York City, NY USA.

Type locality: Biscayne Bay, Florida USA.

Etymology: *acetophilum* is Latin for acetate loving.

Light Microscopy

Aurantiochytrium acetophilum had numerous life stages that were reliably reproduced by manipulating the culture medium and inoculation times with test tubes or flasks; however, the times varied with agitation, nutrients, oxygen content and so forth. Cells grown in stationary test tubes required longer time periods than those placed on a shaker at 180 revolutions per minute (rpm), and the order of stages varied between stationary and agitated cultures. When cells were grown on pine pollen, the stages varied in a third way. Additional culturing techniques were not attempted. Most observations

were carried out using cultures maintained with stationary test tubes, and all the stages described below were observed using this single method.

Sporogenous cells. A test tube culture, regardless of age, that was repeatedly inoculated into fresh medium every 24 h, produced rapidly dividing cells (Fig. 1). The rapidly dividing cells often formed parenchymatous-like masses (Fig. 1A). We termed these masses "sporogenous cells" because cells gave rise to zoosporangia and amoebosporangia. The size of sporogenous cells varied greatly, from 4 to 20 μm; the protoplasm of these cells was quite thin (devoid of lipid granules), and nuclei were distinct (Fig. 1A, B). A few non-sporogenous cells sometimes remained, and these had birefringent storage lipids (Fig. 1A, arrow). Some sporogenous cells had large vacuole-like structures (Fig. 1A, x). Sporogenous cells often had more than one nucleus, indicating that mitosis was occurring more rapidly than cytokinesis. Smaller sporogenous cells had several fates (i.e. growth and division, zoosporangium formation, amoeba formation or amoebosporangium formation) whereas the larger cells were destined to divide repeatedly to produce smaller cells. Rapidly dividing cells frequently produced tetrads of cells that appeared as four pyramid-shaped cells although unless severely flattened by the coverslip, only three cells were visible in one focal plane (Fig. 1B). These cells often were preparing for another round of division and they had four nuclei, which likewise were not always visible in one focal plane (Fig. 1B, arrows). Once the period of rapid cell division ceased, approximately 12 h after inoculation into fresh medium, ectoplasmic nets began to develop (Fig. 1C–E). We were unable to demonstrate that the ectoplasmic nets developed from a single cell site (e.g. brothrosome), but we found that the amount of ectoplasmic net material increased over time in static cultures. Ectoplasmic nets sheared off under heavy mixing and were rarely visible in shake-flask cultures.

Sporangium development. Sporogenous cells began producing Type I sporangia after approximately 6 h after inoculation into new medium (Fig. 2, Supplementary Materials Video S1). The Type I sporangium matured within approximately 0.5–1.0 h and started releasing zoospores or amoebae (see below). Type I sporangia formed as sporogenous cells underwent a series of rapid divisions without noticeable growth (Fig. 2A). Nuclei were very prominent, and cells were often multinucleate, i.e. nuclear division occurred more quickly than cytokinesis (Fig. 2A). Cytokinesis of the multinucleate sporangium mother cell proceeded with either equal (not shown) or unequal divisions (Fig. 2A). The rapid cell division then produced a sporangium with 8–32 cells (Fig. 2B, C). Sporangia with fewer than eight cells were never observed, and 32-celled sporangia were uncommon.

Type II sporangia had a large multinucleate cell that "pinched off" spore cells around its periphery (Fig. 2D, Supplementary Material Video S2). The spore cells appeared to be formed within the large central cell and were squeezed outside (Fig. 2D, arrows). When fully formed, a Type II sporangium still had the large central cell and 32 peripheral spores (Fig. 2E-F). The peripheral cells surrounded the entire surface of the central cell, i.e. they were not a ring-like structure (Supplementary Material Video S2). The spore cells were about 3–5 μm in diameter, and they gave rise to small, spherical swimming cells. Type II sporangia were quite distinct but very rarely formed, and they were not fully investigated.

Sporangia with other shapes were also formed but were probably variants of the Type I sporangium. In some cases, the sporangial cells were attached in the center, much like the cells of *Synura* (Fig. 2G). Sporangia formed on pollen grains had a heavy wall as the spore mother cell developed (Fig. 2H). Some sporangia developed as an amorphous shape with irregular division to produce spore cells (Fig. 2I).

Zoospore formation. Zoosporangia produced 8, 16 or 32 biflagellate zoospores (Figs 3, 4, Supplementary Material Video S1). The serial development of Type I zoosporangia was captured in one image (Fig. 3A, arrowheads). The spore cells of the sporangium gradually produced flagella and as the flagella developed, the sporangium (or cluster of zoospores) began to swim (Fig. 3B). The cluster of cells constantly moved and it was difficult to follow flagellar development (Supplementary Material Video S1); however, it appeared that the anterior (=immature) flagellum developed first, retracted and then both the anterior and posterior (=mature) flagella appeared. The flagellar "colony" of zoospores did not swim in a directed motion, rather it erratically bounced around as the zoospore flagella pulled in random directions. The shape of the zoospores was highly irregular while they were attached together, but they tended to be elongate and slightly rectangular in outline (Fig. 3B–E, Supplementary Material Video S1). Cells in Type I sporangia were sometimes attached to each other by a cytoplasmic strand that extended between two or more cells (Fig. 3D–I). The zoospore escaped the cluster by twisting, pulling and rotating until the cytoplasmic strand broke or dissolved. No single pattern of zoospore release was observed.

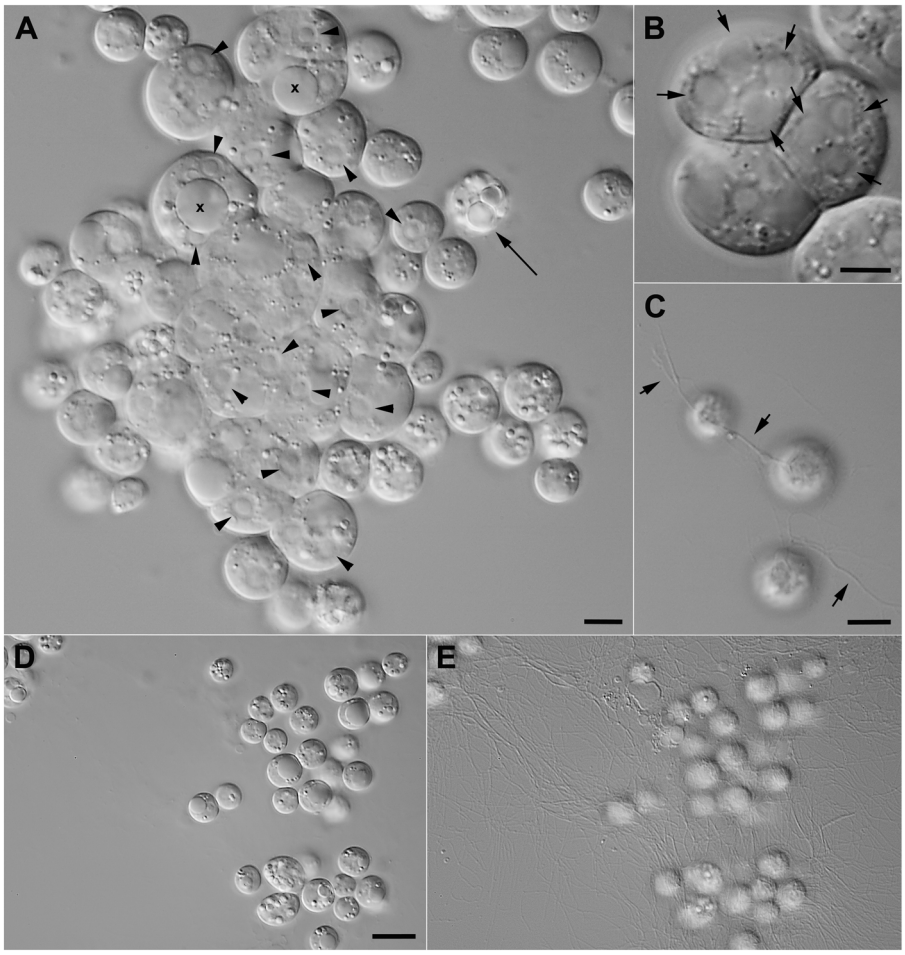

Figure 1. Sporogenous cells and ectoplasmic nets. **A**. A mass of sporogenous cells showing the numerous nuclei (arrowheads) and a more typical vegetative cell with large lipid granules (arrow). Note the large vacuole-like bodies of unknown function (x). Scale bar = 5 μm. **B**. A tetrad of sporogenous cells (three visible cells) undergoing rapid cell division. Note the prominent nuclei (arrows). Scale bar = 5 μm. **C**. Sporogenous cells with early development of ectoplasmic nets (arrows). Scale bar = 5 μm. D, E. Two focal planes of a sporogenous cell mass showing the extensive development of ectoplasmic nets. Note that the ectoplasmic nets originate numerous times from some cells. Scale bar = 10 m.

For example, one cell broke its strand and separated from the zoospore cluster (Fig. 3D), but then its posterior flagellum became attached to the cluster for at least one minute (Fig. 3E). One three-celled group was swimming around for over five minutes while attached by tri-radiate cytoplasm strand (Fig. 3F–G). The spinning motion of this triad was apparent from the position of the biflagellate cell anterior flagellum (Fig. 3F–H, arrowheads). As the three cells moved, different views of the tri-radiate cytoplasmic strand were shown (Fig. 3F–H, arrows). Flagella were still developing during the early developmental process, as evidenced by the blubs on the ends of flagella (Fig. 3I, arrowheads).

Zoospore morphology. Type I biflagellate zoospores were irregular in shape when attached in a zoospore cluster (Fig. 3), but they became pyriform-shaped when freely swimming; eventually, they became smaller and spherical in shape (Fig. 4). A pyriform zoospore with fully-developed anterior and posterior flagella still had a bit of cytoplasmic connecting material (Fig. 4A). These zoospores were most common, and they had a flattened, slightly indented area where the flagella were attached. We also observed uniflagellate zoospores, but these were uncommon (Fig. 4B, C). One cell was clearly undergoing flagellar transformation and the immature flagellum was ready to retract (Fig. 4B). The flagellar base was

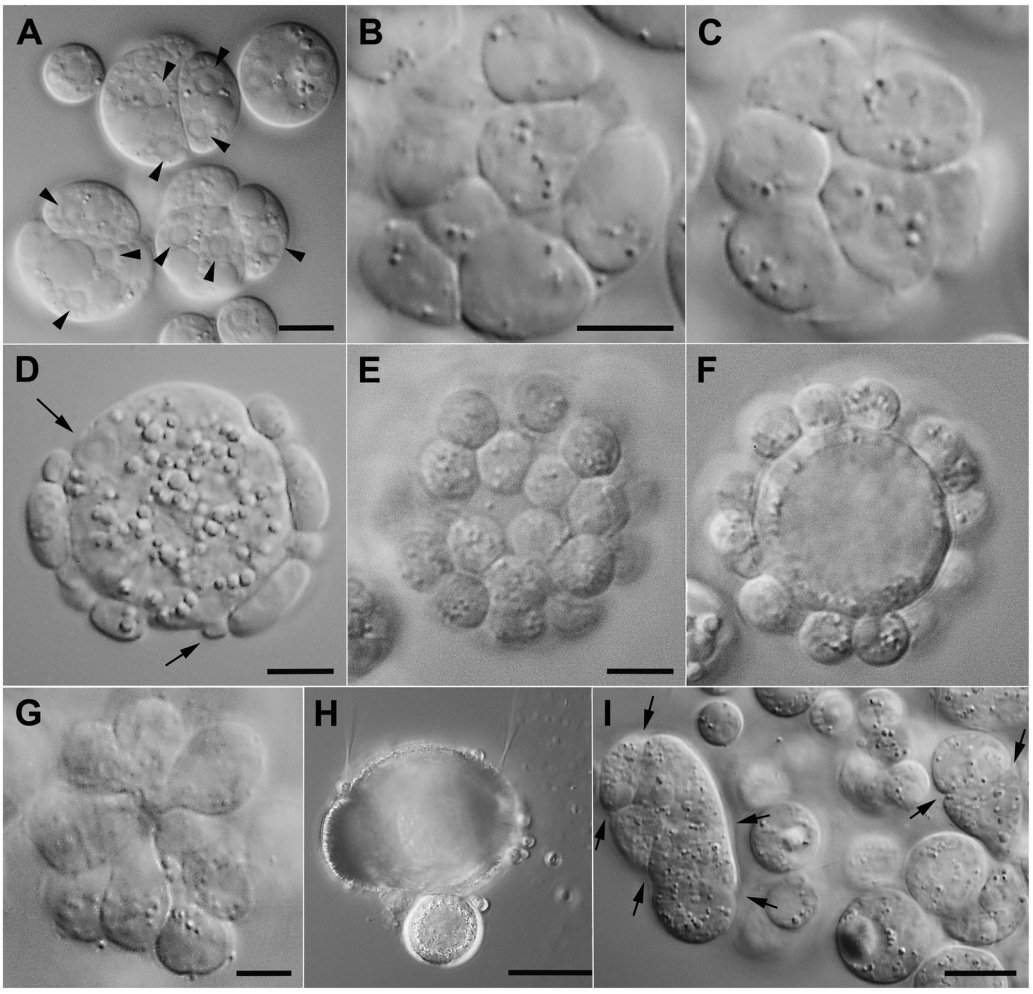

Figure 2. Sporangium development. **A**. Early sporangia that differ from rapidly dividing sporogenous cells by their unequal cell divisions. Note the prominent nuclei. Scale bar = 5 μm. **B, C**. Bottom and top optical views of a 16-cell Type I sporangium. Scale bar = 5 μm. **D**. Possible early development of a Type II sporangium. Note the large central cell, the peripheral spore cells and the budding formation of new spore cells (arrows). Scale bar = 5 μm. **E, F**. Two focal planes of a Type II sporangium showing the peripheral spore cells and the large central cell. Scale bar = 5 μm. **G**. An unusual Type I sporangium where the cells are attached in the center and cells radiating out like a *Synura* colony. Scale bar = 5 μm. **H**. A sporangium formed on a pine pollen grain. Note the spores from other sporangia. The filaments were formed by bacteria. Scale bar = 30 μm. **I**. Two early developing and irregularly forming sporangia. Note the unequal cell divisions identifiable from the cleavage planes (arrows). Scale bar = 10 μm.

adjacent to the nucleus (Fig. 4B, arrowhead). A second uniflagellate cell was irregularly shaped and its developmental stage could not be determined (Fig. 4C). A pyriform cell and spherical cell were probably from different origins, but they were attached by the posterior flagellum of the spherical cell (Fig. 4D arrowhead). The spherical cell is smaller. Finally, a fully matured spherical cell was even smaller, it had a distinctly obvious nucleus and it had very few or no lipid granules (Fig. 4E).

The anterior flagellum beat with a sinusoidal wave and it pulled the zoospore forward; the posterior flagellum beat with a stiff sculling motion, like that of a single oar placed at the aft of a boat, and this motion pushed the cell forward (Fig. 4F–J, Supplementary Material Video S3). When viewed from the top of the cell, the anterior flagellum was inserted slightly to the left of the posterior flagellum insertion (Fig. 4F, arrowheads). Although more obvious in pyriform shaped zoospores, this spherical zoospore had a slight trough-like depression

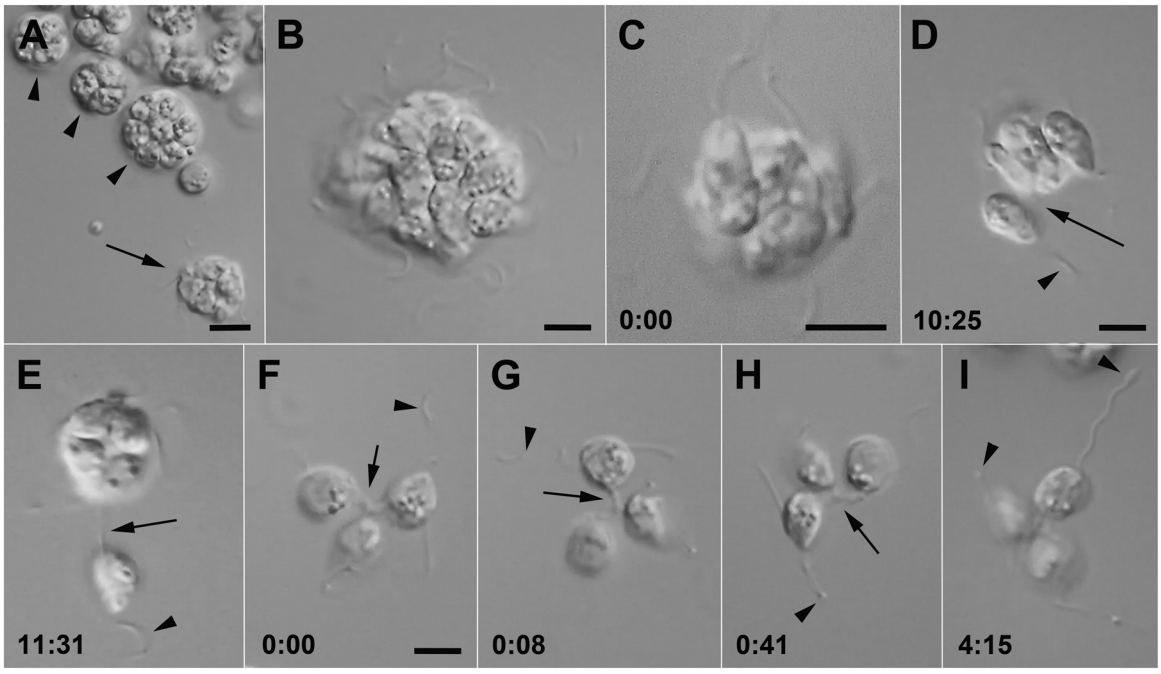

Figure 3. Zoosporangia. **A**. A zoosporangium with developing flagella (arrow) as well as three future zoosporangia (arrowheads). Scale bar = 5 μm. **B**. A 32-cell sporangium with developing flagella. Scale bar = 5 μm. **C–E**. An 8-cell zoosporangium over time as zoospores become free. Scale bar = 5 μm. **C**. Irregular, box-like zoospores. **D**. The anterior flagellum (arrowhead) and an attachment (arrow) to sporangium. Scale bar = 5 μm. **E**. Further release of the zoospore with attachment by the posterior flagellum (arrow). Note the anterior flagellum (arrowhead). See D for scale bar. **F–I**. A three-cell cluster of zoospores broken away from a larger zoosporangium. Scale bar = 5 μm. **F**. Zoospores held together by triangular cytoplasmic strands (arrow). The anterior immature flagellum of one cell is shown (arrowhead). **G**. The zoospores rotated 90° in eight seconds. The cytoplasmic strand is clear (arrow); same flagellum as F (arrowhead). **H**. Cells rotated again approximately 90° in 33 seconds. The long anterior flagellum appears to be bulbous, but these are flagellar coils (arrowhead). **I**. Two flagella have bulbs (arrowheads) at the ends of flagella.

beneath and to the right of the anterior flagellum (Fig. 4F–J). The zoospores swam for perhaps 0.5–1.0 h, settled, attached to a surface, and then grew and divided.

Amoeba formation. The formation of amoebae generally occurred after the first round of zoosporangia were formed by the sporogenous cells. Like zoospores, they were formed in various ways. Sometimes the amoebosporangium superficially resembled the Type II zoosporangium, and amoebae separated and moved away by amoeboid action (Fig. 5A). Other times, masses of eight cells suddenly transformed into amoebae (Fig. 5B; Supplementary Material Video S4). Single spherical cells, destined to be amoebae, formed a bubble-like protrusion and the cytoplasm flowed out into an amoeba (Fig. 5C, Supplementary Material Video S5). Amoebae produced short, fine unbranched or branched filament-like structures from the main amoeba body, and these could be extensive on some amoebae (Fig. 5D). Amoebae were generally linear or block-shaped (Supplementary Material Fig. S1), and they never showed fine radiating rhizopodia such as for *Actinophrys*.

The formation of amoebae from sporogenous cells was documented using time-lapse photographs and a hanging drop preparation (Supplementary Material Figs S2–S6). Ten cells or cell clusters were chosen and numbered (Supplementary Material Fig. S2A). Cell 1 was positioned near a developing zoosporangium, and when the zoosporangium began swimming, Cell 1 was pushed out of the photographic frame (Supplementary Material Fig. S2B). Cell 10 had already divided into eight cells and these were labeled a–h (Supplementary Material Fig. S2C). Normally, the eight cells were a sporangium and produced either zoospores or amoebae. But the eight cells remained spherical (Supplementary Material Fig. S2D), and these cells followed different patterns (see Cell 10 below). Cell 5 produced an eight-cell sporangium, and Cell 3 divided into four cells (Supplementary Material

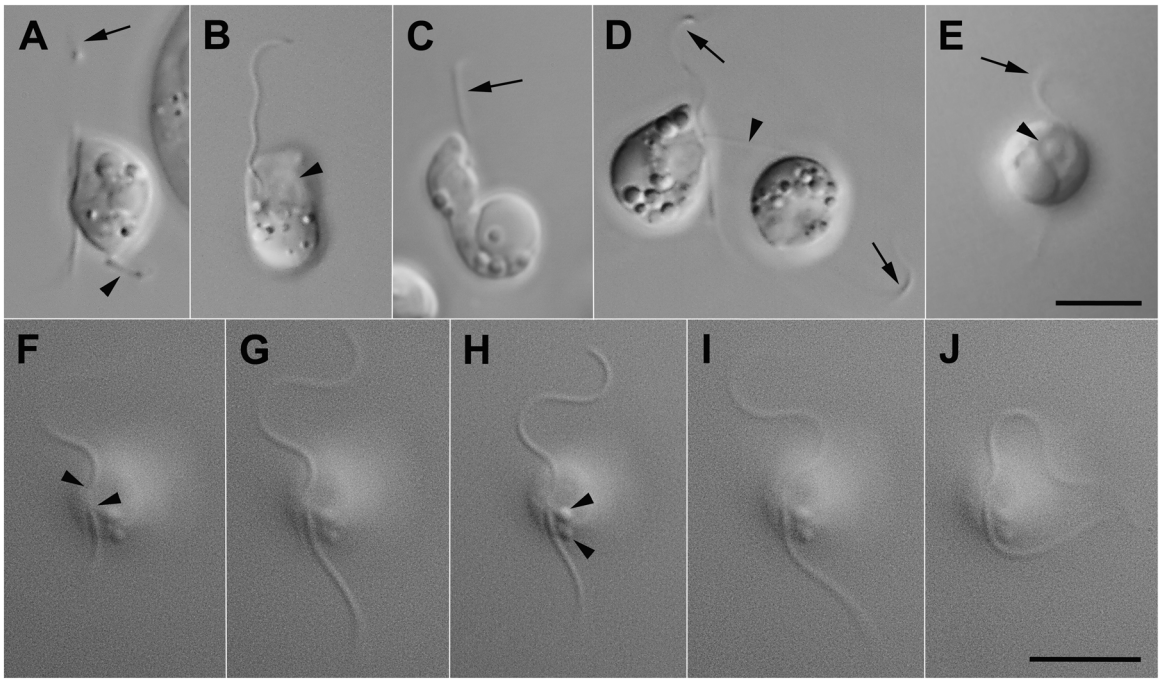

Figure 4. Swimming cells. Anterior mastigoneme-bearing flagellum is always oriented toward the top of the page; the posterior flagellum is oriented toward the bottom of the page. **A–E**. Scale bar = 5 μm. **A**. Somewhat pyriform zoospore with anterior flagellum (arrow), posterior flagellum and the remnants of an attachment piece (arrowhead). **B**. Uniflagellate cell, presumably beginning flagellar transformation. Note the obvious nucleus (arrow). **C**. Odd uniflagellate cell; anterior flagellum is indicated by arrow. **D**. Pyriform cell (left) and spherical cell (right). Both have two flagella and no cytoplasmic attachment; the cells are held together by the posterior flagellum (arrowhead) of the spherical cell; the anterior flagella are indicated (arrows). **E**. Small, spherical cell with obvious nucleus and nucleolus (arrowhead). The anterior flagellum (arrow) is rather short and this might possibly be a gamete. **F–J**. Single swimming cell showing flagellar insertion and beating patterns. Scale bar = 5 μm. **F**. Flagellar insertion is shown for the anterior flagellum (left arrowhead) and posterior flagellum (right arrowhead). **G**. Anterior flagellum with a sinusoidal wave, posterior flagellum stiff. **H**. Two spherical structures near the base of the posterior flagellum (arrowheads). **I, J**. Beat patterns of flagella.

Fig. S2). Two unnumbered sporogenous cells were captured before they matured directly into amoebae (Supplementary Material Fig. S3C, arrows). Once these cells became amoeboid (Supplementary Material Figs S3D, S4B – see inset images), they moved around the sporogenous cell mass for a short time and then disappeared into the medium of the hanging drop. Other single sporogenous cells also converted directly into amoebae (Supplementary Material Fig. S4D).

A cluster of cells appeared in the upper right corner (Supplementary Material Fig. S4A) and moved along an ectoplasmic net strand (Supplementary Material Fig. S4D). Unfortunately, the microscope slide was slightly repositioned during the intermediate times (Supplementary Material Fig. S4B, C), but it was visible at the top of Supplementary Material Figure S5A. A second cluster of cells, an amoebosporangium, was observed sliding along the ectoplasmic net strand (Supplementary Material Fig. S5A–C, see extreme right side and arrowhead position markers). The ectoplasmic net strand used by the first moving cluster of cells was also used by this second cell cluster (Supplementary Material Fig. S5B–C, small open arrowheads).

Over time, more single sporogenous cells converted directly to amoebae (Supplementary Material Fig. S5A, B small arrows). Cell 6 divided into four cells (Supplementary Material Fig. 5SB, large arrow) and Cell 8 divided into four cells (large arrowhead). Cell 9 divided into eight cells that became amoebae (Supplementary Material Fig. S5C, arrow). One of the daughter cells from Cell 5 became an amoeba (Supplementary Material Fig. S5E, arrowhead), and one cell from moving sporangium became amoeboid (Supplementary Material Fig. S5E, arrow). Both of these amoebae formed from a tongue-like protuberance that

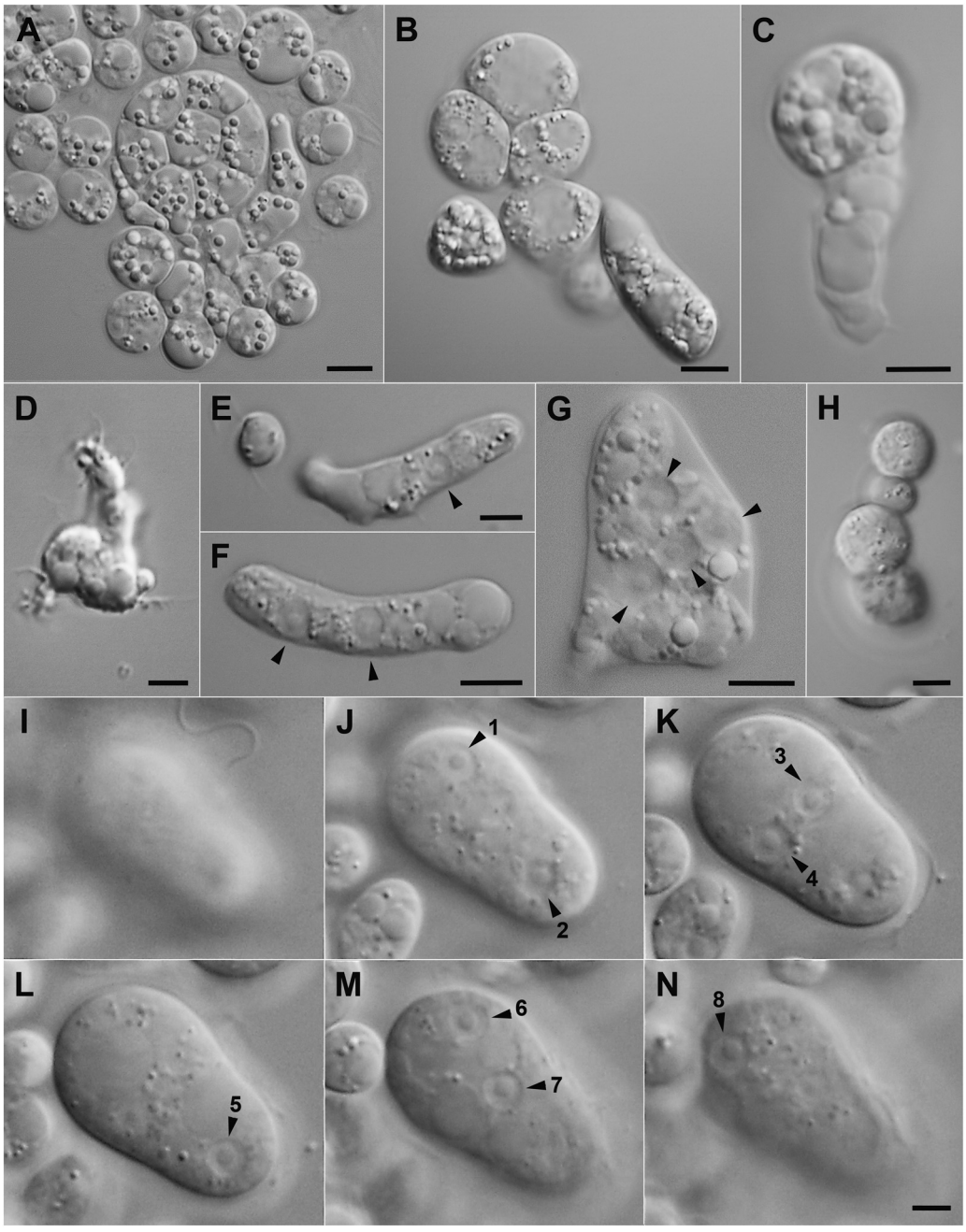

Figure 5. Amoebosporangia and amoebae. Scale bars = 5 μm. **A**. Sporogenous cells forming an amoebosporangium that is releasing amoeba cells. **B**. Eight-celled sporangium rapidly converting into independent amoeba cells. **C**. Amoeba forming from a spherical cell. **D**. Amoeba with numerous fine, finger-like pseudopodia. **E**. Linear amoeba with a single nucleus (arrowhead). The spherical cell is a zoospore. **F**. Linear amoeba with two nuclei (arrowheads). **G**. Block-like amoeba with four nuclei (arrowheads). **H**. Amoeba that divided into four cells arranged in a linear pattern. **I–N**. Amoeba with eight nuclei photographed at different focal planes. The eight nuclei are numbered and indicated with arrowheads.

pushed out from a spherical cell. Another daughter cell from Cell 5 was large (Supplementary Material Fig. S5F, arrow) and then underwent rapid divisions (less than 20 minutes) to produce eight cells that eventually became amoebae (Supplementary Material Fig. S5G, arrow).

The eight cells labeled a–h that were produced from Cell 10 (see Supplementary Material Fig. S2C) each produced an amoeba or an amoebosporangium (Supplementary Material Fig. S6). Cell 10d, from the original Cell 10, divided into two cells (Supplementary Material Fig. S5B, double arrowheads) and they were converted into amoebae (Supplementary Material Fig. S5C, arrow). Cell 10g divided into four cells (Supplementary Material Fig. S5C, arrowhead). Cell 10 c divided into four cells (Supplementary Material Fig. S6A: cells c1, c2, c3 are visible in this focal plane). Cells 10f, 10g and 10h each divided to produce 8-celled amoebosporangia (Supplementary Material Fig. S6A). The amoebosporangium of Cell 10f produced amoebae (Supplementary Material Fig. S6B, C, D). One amoeba from the Cell 10g amoebosporangium was captured on an image (Supplementary Material Fig. S6E), and the amoebosporangium from Cell 10h produced amoebae (Supplementary Material Fig. S6F). In summary, Cell 10 was a sporogenous cell that divided into 8 "vegetative" cells, some of the eight cells converted directly into amoebae, and some of the cells produced amoebosporangia that in turn produced amoebae. Ultimately, the amoebae moved out of the plane of focus (into the hanging drop) and were not observed again.

Some larger amoebae became multinucleate. The first indication that the amoeba would become multinucleate was when the nucleus and nucleolus became prominent (Fig. 5E). Most commonly, the multinucleate amoebae were linear (Fig. 5E, F), but some were more block-like in shape (Fig. 5G). The four nucleate amoebae either divided into four spherical cells (Fig. 5H) or the amoeba rounded up to a single spherical cell (not shown). In both cases, the nuclei were no longer prominent. The fate of the single spherical cell was not determined, and it is not known if the nuclei fused or if the cell produced four daughter cells. One eight-nucleate amoeboid-like cell was photographed (Fig. 5I–N), but its origin and its fate were not observed.

Vegetative cells. Vegetative cells differed from sporogenous cells because they grew in size, often had a thin, visible cell wall, and had numerous lipid bodies (compare Fig. 6A and B–D). Unlike sporogenous cells, vegetative cells were simultaneously dividing and accumulating lipids (Fig. 6E). Vegetative cell division occurred within the mother cell wall and daughter cells were temporarily held together (Fig. 6E). Vegetative cells were responsible for the bulk of the lipid production regardless of culture method (Fig. 6B–E). For well-aerated commercial cultures, only vegetative cells occurred after 16 h beyond inoculation. At the end of a commercial batch, vegetative cells were filled with lipids and they remained buoyant when placed in seawater.

Cysts. Cells of any type, when placed for weeks in a culture medium lacking the medium nutrients, gradually produced thicker cell walls (Fig. 6C–H). The walls were both stratified (Fig. 6C, D, G) and unstratified (Fig. 6E, F, H). Vegetative cells in tetrads could form thick walls (Fig. 6E), and even sporangia were able to form a wall layer (Fig. 6F). The consistency of the cytoplasm varied and seemed to be unrelated to the wall type (stratified or unstratified). Some cells appeared to have subdivisions (Fig. 6D, H). Even after several weeks, lipids were not mobilized or used by the cell despite the organic carbon limiting conditions. Furthermore, we observed that excysting and subsequent lipid mobilization were only triggered when the nitrogen, phosphorous and sulfates were restored, regardless of the presence organic carbon source. Consequently, we distinguished these heavily walled cells as cysts, which represented the resting stage of the organism.

Sexual reproduction. Huge numbers of swimming cells were produced when sporogenous cells were transferred to L1 medium (salinity = 32), and they were mostly formed from Type I sporangia. However, no morphological features distinguished zoospores from putative gametes, and we were unable to separate the two zoosporangium types by isolation, post-inoculum timing or environmental conditions. Therefore, we did not determine the fate of swimming cells from Type II sporangia.

Swimming cells from strain HS-399 appeared to pair together, but this was inclusive (Supplementary Material Fig. S7). There was cytoplasmic fusion, but we could not demonstrate nuclear fusion. Nevertheless, this observation possibly suggested a homothallic type of sexual reproduction. We observed pyriform cells paired together with smaller round cells, but when trying to demonstrate nuclear fusion (i.e. zygote formation), these attempts failed (Supplementary Material Fig. S8).

A drop of HS-399 (or of HS-412, a second isolate from the same field collection as HS-399) on an uncovered microscope slide showed no pairing of cells. When HS-399 and HS-412 were combined, numerous paired cells were observed (Supplementary Material Video S6, segment H). The pairing of two swimming cells occurred immediately upon

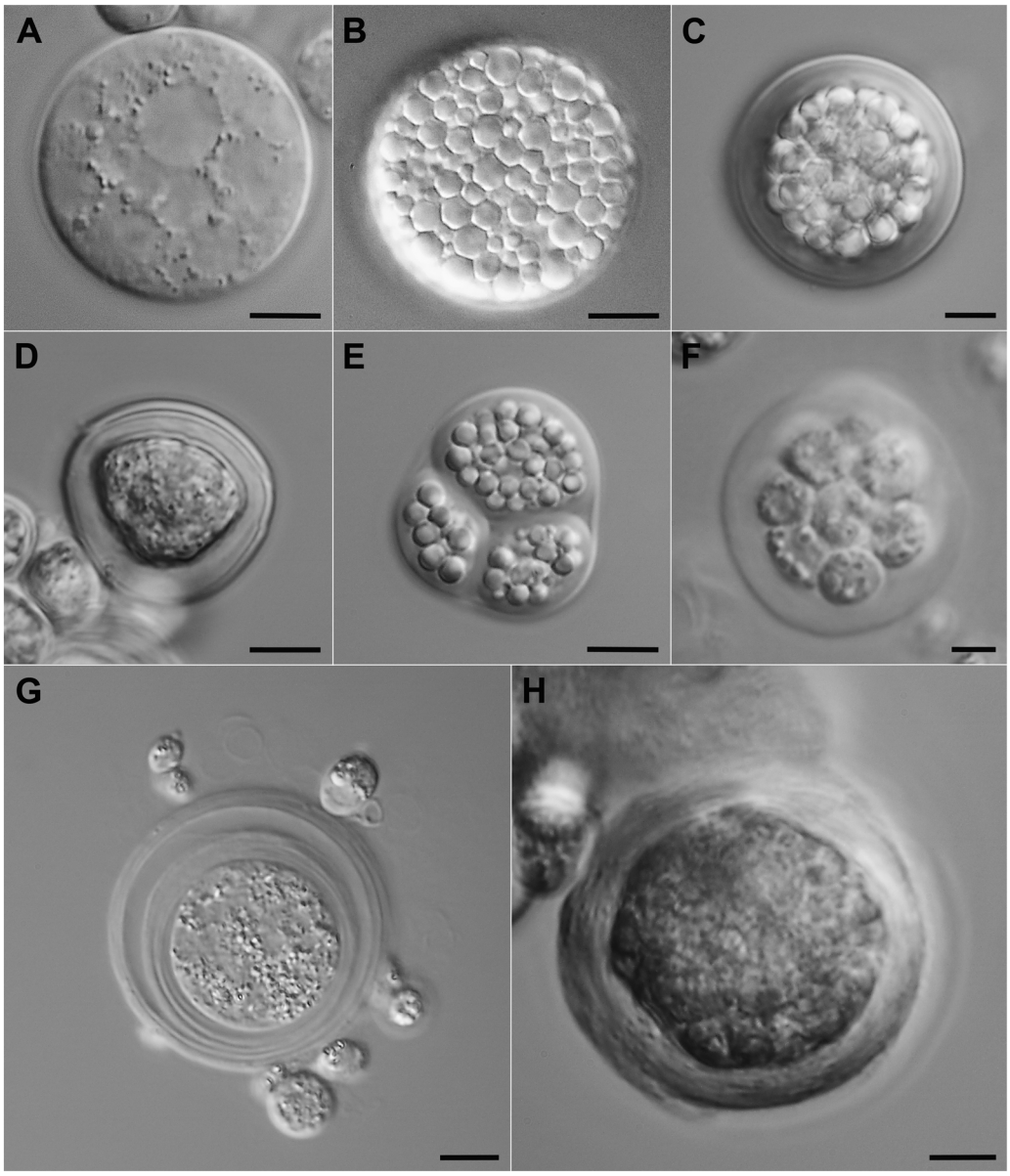

Figure 6. Cell walls and cysts. Scale bars = 5 μm. **A**. Typical large sporogenous cell without any obvious cell wall. **B**. Stationary phase cell filled with lipid granules; there is no obvious cell wall. **C**. A Stationary phase cell filled with lipid granules. Note the stratified cell wall. **D**. A cell without lipid granules with a distinctly stratified wall. **E**. Three of four cells with lipid granules and with cell walls around the tetrad and around individual cells. **F**. A sporangium (probably 16-celled) with a thick wall. **G**. A large sporogenous cell that produced a thick stratified cell wall. Note the attached swimming cells. **H**. A cell or sporangium (unclear) with a thick wall.

mixing, before the slide was in place and the video camera was started. Paired cells attached on the cell surface opposite to their flagella (i.e. dorsal surface) and they continued to swim after pairing (Fig. 7). One pair was followed from early pairing to cytoplasmic and nuclear fusion using different magnifications (Fig. 7, Supplementary Material Video S6). The attached pair of cells swam together for a short time, and then one cell began to cast off its flagella; the other cell remained swimming for a few minutes longer (Fig. 7A–E). There was a terminal flagellar swelling that suggested the cell was attempting to retract the flagellum (Fig. 7E). As the cytoplasm began to connect between the two cells, the remaining flagella were cast off and the cytoplasm flowed into a single cell (Fig. 7F–J). At higher

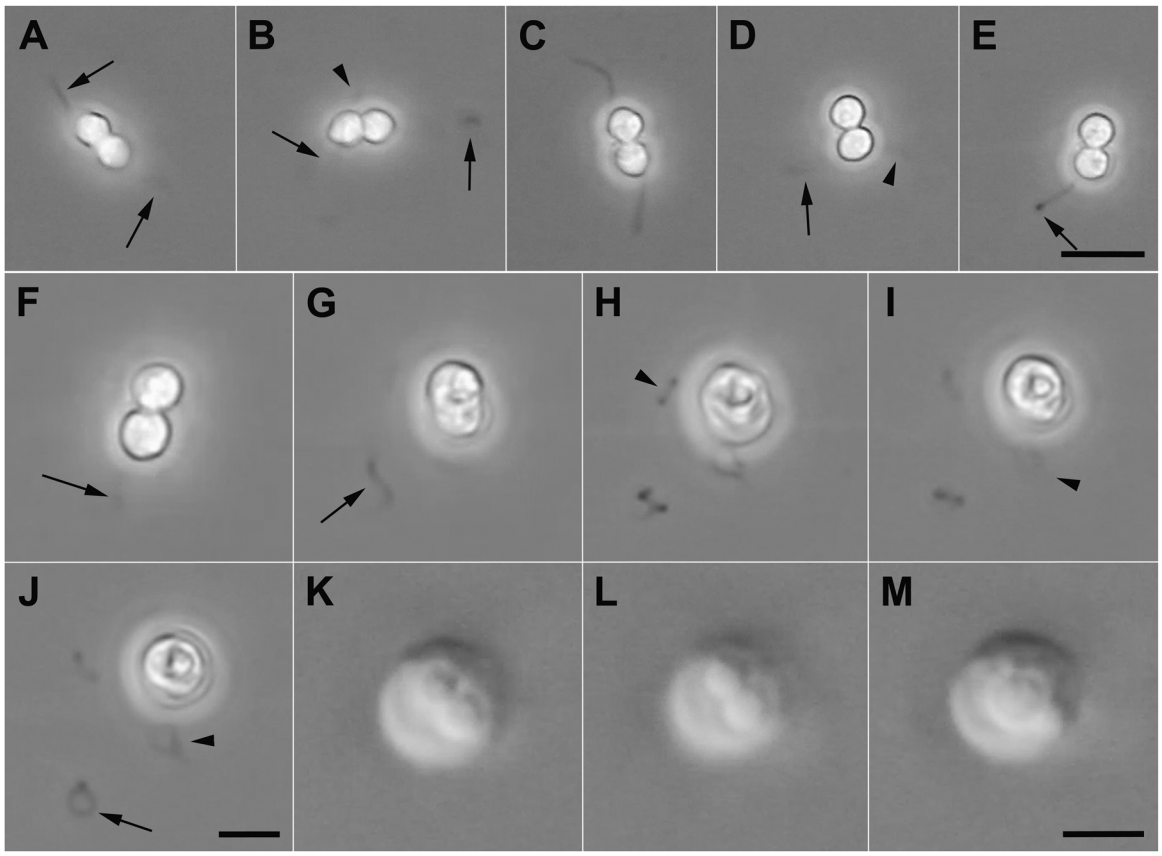

Figure 7. Sexual fusion between gametes of strains HS-399 and HS-412. Video was captured at three different magnifications. Scale bars = 5 μm. **A–E**. Low magnification showing the paired cells as they rotate while swimming. **A**. The anterior flagella of the two gametes are indicated (arrows). **B**. The posterior flagellum on one gamete is indicated (arrowhead). **C**. Two anterior flagella clearly visible. **D**. Anterior (arrow) and posterior (arrowhead) flagella of one gamete. **E**. Balled end of the flagellum indicating a cellular retraction of the flagellum (arrow). **F–J**. Intermediate magnification. Flagella being cast off. **F**. Anterior flagellum intact (arrow). **G**. Anterior flagellum cast off (arrow). **H**. Posterior flagellum cast off; anterior flagellum (arrow) and posterior flagellum (arrowhead) are still visible. **I**. Flagellum of one gamete still attached. **J**. Flagellum of second gamete cast off. **K–M**. Enlarged view of two nuclei fusing. **K**. Rounded cell with unfused nuclei. **L**. Nuclei beginning to fuse. **M**. Nuclei fused into one nucleus.

magnification, the two nuclei were observed to fuse into a single nucleus (Fig. 7K–M). The fate of this putative zygote could not be followed because the "zygote" was not recovered from the hanging drop preparation.

We carried out other experiments while investigating sexual reproduction. For example, filtered medium from a culture of one strain having many swimming cells both did and didn't influence the swimming cells of a second strain. That is, sometimes the swimming cells dramatically increased their swimming speed, but when the experiments were repeated on other days, there was no apparent change in swimming speed. Therefore, a pheromone-type molecule might be present at times, but no conclusive evidence was obtained. We also tested favorable conditions (e.g. fresh *Aurantiochytrium* medium) and unfavorable conditions (e.g., seawater without nutrients; low salinities using distilled H_2O). There was no definitive indication that these environmental conditions influenced sexual reproduction, but as mentioned above, huge numbers of swimming cells were produced when sporogenous cells were placed in L1 medium (salinity = 32). Finally, extracts from mangrove leaves, temperature changes and additions of various organic substrates provided no further insights regarding sexual reproduction.

Life cycle. A partial life cycle was determined for *Aurantiochytrium acetophilum* (Fig. 8). Morphological stages had discrete paths of development, but these paths often had options. The most versa-

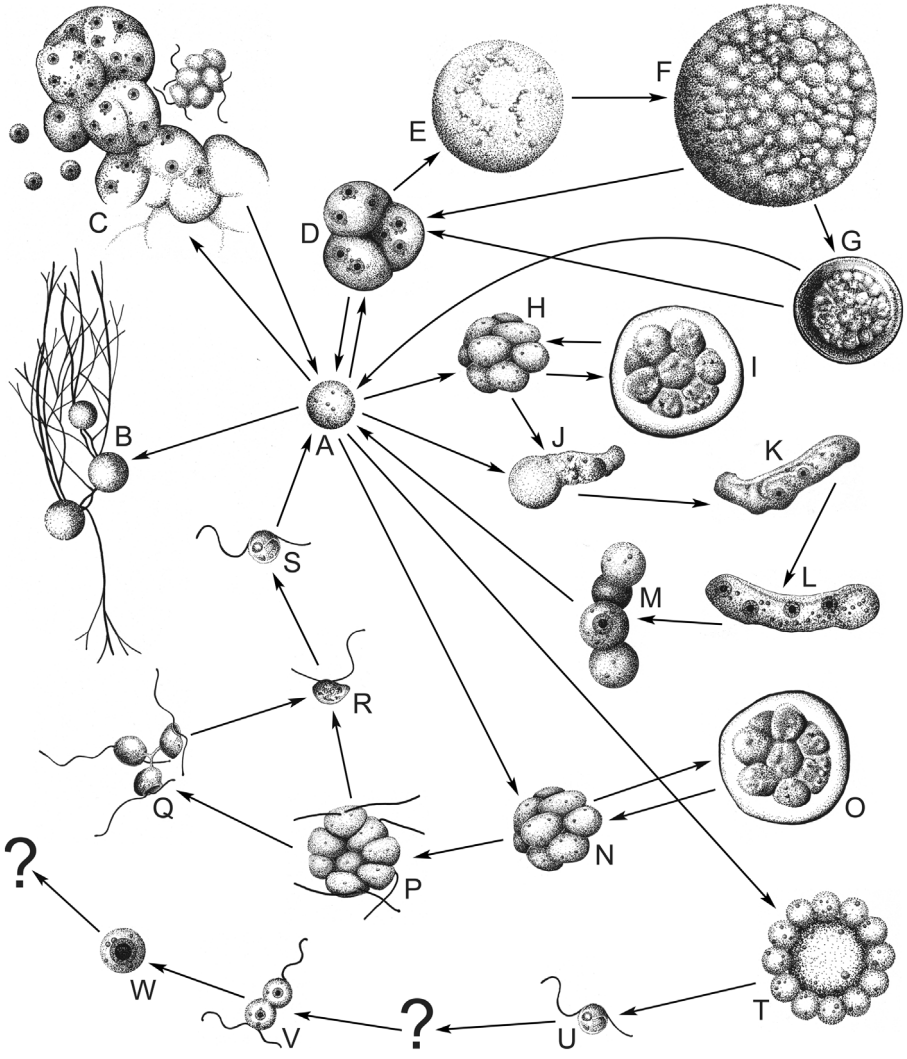

Figure 8. Life cycle of *Aurantiochytrium acetophilum*. **A**. Typical small sporogenous cell. **B**. Vegetative cells with ectoplasmic nets. **C**. Sporogenous multinucleate cell mass producing small sporogenous cells and a Type I sporangium. **D**. Tetrad of multinucleate sporogenous cells. **E**. Typical large vegetative cell before filled with lipids. **F**. Large oleaginous cell. **G**. Cyst. **H**. Amoebosporangium. **I**. Encysted amoebosporangium. **J**. Amoebospore transforming into an amoeba. **K**. Binucleate amoeba. **L**. Quadranucleate amoeba. **M**. Four uninucleate amoebospores. **N**. Type I zoosporangium before flagella formation. **O**. Encysted zoosporangium. **P**. Type I zoosporangium with flagellate cells. **Q**. Three zoospores connected by a cytoplasmic band. **R**. Younger single pyriform zoospore. **S**. Older single spherical zoospore. **T**. Type II sporangium. **U**. Small spherical swimming cell (gamete?). **V**. Initial fusing of two motile gametes. **W**. Uninucleate zygote.

tile stage was a single cell that lacked an obvious cell wall and had little or no lipid granule accumulation. As described above, there was evidence that pointed to sexual reproduction, but the fate of the putative zygote was not determined and the stage involving meiosis was not identified.

Transmission Electron Microscopy

Stationary cells were packed with lipid granules, but due to fixation and dehydration problems, fine details at high magnification were not possible (Fig. 9A). Sporogenous cells were better pre-

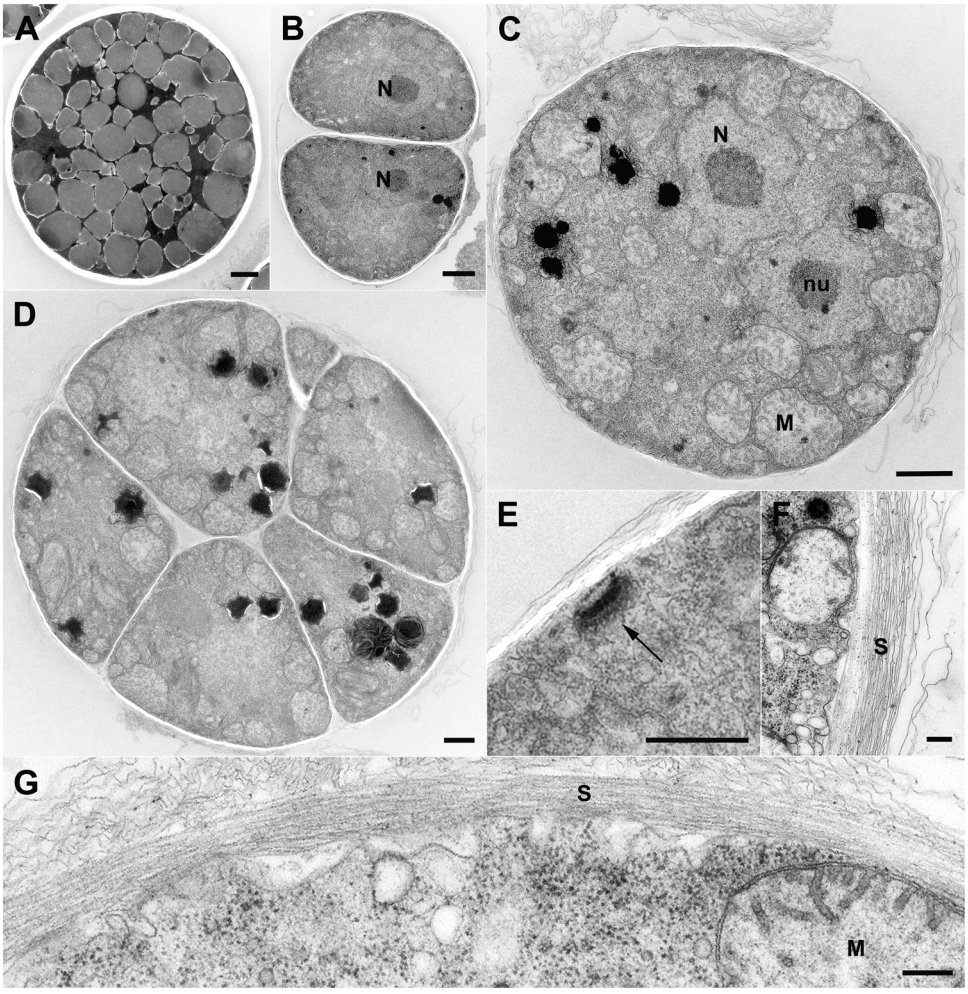

Figure 9. Transmission electron microscopy. **A**. Cell filled with lipid granules. Slight contraction during dehydration to leave clear or empty area around the cell. Scale bar = 2 μm. **B**. Recently divided cells showing distinct nuclei (N) with dense nucleoli. A fine scale wall can be seen on the left side. Scale bar = 1 μm. **C**. A sporogenous cell with peripheral mitochondria (M). Nucleus (N), nucleolus (nu). Scale bar = 1 μm. **D**. Sporangium showing wedge-shaped cells. Scale bar = 1 μm. **E**. A bothrosome-like structure (arrow). Scale bar = 500 nm. **F**. Scale layer (S) forming the cell wall. Scale bar = 200 nm. **G**. Enlarged scale layer (S). Note the peripheral mitochondrion (M). Scale bar = 200 nm.

served (Fig. 9B–E). Recently divided sporogenous cells had prominent nuclei with dense nucleoli (Fig. 9B). Predivision sporogenous cells were multinucleate and numerous mitochondrial profiles were observed around the periphery of the cells (Fig. 9C). Sporangia were rarely sectioned but appeared similar to sporogenous cells with regard to cellular contents (Fig. 9D). Cells had large Golgi bodies, extensive endoplasmic reticula, numerous mitochondrial profiles, and occasional lipid granules (not shown). One brothrosome-like structure was observed but there was no evidence of ectoplasmic net formation by this sporogenous cell (Fig. 9E). Vegetative cells, which were not yet accumulating large amounts of lipids, had a cell wall formed from scales (Fig. 9F, G). The origin of the scales (e.g. from Golgi vesicles) was not determined. The surface view of individual scales was not observed.

Lipids and Substrate Assimilation Profiles

When *Aurantiochytrium acetophilum* HS-399 and *Aurantiochytrium limacinum* (D.Honda & Yokochi) Yokoyama & D.Honda strain SR21 were grown under identical conditions, both strains reached stationary phase after four days incubation with 30–40 g CDW/L (Fig. 10); however, *A. acetophilum*

Table 1. Total lipids and fatty acid profiles for *Aurantiochytrium acetophilum* strain HS-399 and *Aurantiochytrium limacinum* strain SR21 following 120 h incubation in glycerol.

	Aurantiochytrium acetophilum HS-399	*Aurantiochytrium limacinum* SR21
Total lipids (% DW)	84.0 ± 1.0	74.3 ± 0.6
Total fatty acids (% DW)	73.4 ± 1.0	60.2 ± 2.0
Fatty acid profile (% TFA)		
14:0	2.3 ± 0.1	2.4 ± 0.0
15:0	0.2 ± 0.0	0.4 ± 0.0
16:0	47.5 ± 0.3	42.5 ± 0.6
18:0	1.4 ± 0.0	1.4 ± 0.0
20:3 (n-6) & 21:0	0.1 ± 0.0	0.9 ± 0.1
20:5 (n-3)	0.0 ± 0.0	0.0 ± 0.0
22:5 (n-6)	7.8 ± 0.1	10.0 ± 0.1
22:6 (n-3)	38.6 ± 0.1	40.1 ± 0.6
Other fatty acids	1.9 ± 0.1	1.9 ± 0.1

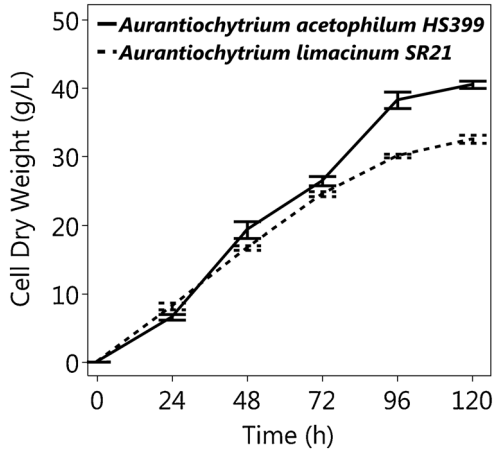

Figure 10. Growth of *Aurantiochytrium acetophilum* HS-399 and *Aurantiochytrium limacinum* SR21 in glycerol.

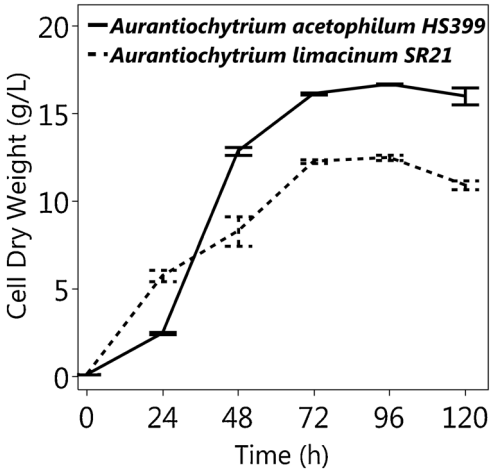

Figure 11. Growth of *Aurantiochytrium acetophilum* HS-399 and *Aurantiochytrium limacinum* SR21 in acetate.

accumulated 13% more lipids and 22% more TFA (% DW) than *A. limacinum* (Table 1). Their fatty acid profiles were very similar with palmitic acid (C16:0) and docosahexaenoic acid (22:6 n-3) accounting for more than 80% of the fatty acids (Table 1). *Aurantiochytrium acetophilum* contained 2.64 mg/kg of astaxanthin esters and 308 μg/kg of beta-carotene, but non-esterified astaxanthin, lutein, zeaxanthin and canthaxanthin were not detected.

The substrate assimilation profiles of *A. acetophilum* and *A. limacinum* were very similar (Table 2). Both strains consumed hexoses but did not assimilate pentoses, disaccharides or longer polysaccharides (Table 2). Both strains also consumed less common carbon sources such as glycerol and acetate. *Aurantiochytrium acetophilum* grew better on acetate than *A. limacinum* (Fig. 11).

Strain HS-399 also demonstrated an extraordinary tolerance to acetate toxicity, growing on acetate as sole carbon source at a pH level as low as 5 without showing any organic acid inhibition (Fig. 12).

Molecular Phylogenetic Studies

Direct sequencing of the 18S rRNA from a monoclonal culture of *Aurantiochytrium acetophilum* (strain HS-399) produced only a few readable pairs, followed by a superimposition of nucleotide bases. The intragenomic sequence heterogeneity was evaluated by cloning and sequencing the 18S rRNA amplicon, which produced 29 distinct paralogs (Genbank accession numbers MH319310-MH319338). An alignment of the paralogs identified 11 distinct zones containing nucleotide insertions or deletions (indels) (Sup-

Table 2. Carbon assimilation profiles of *Aurantiochytrium acetophilum* strain HS-399 and *A. limacinum* strain SR21. Cell biomass produced by each substrate was compared to a negative control (i.e. glutamate was the only substrate) and denoted as a '+' when the biomass produced exceeded the control.

Carbon Source	*A. acetophilum* HS-399	*A. limacinum* SR21
D-glucose	+	+
D-fructose	+	+
D-mannose	+	+
D-galactose	+	+
Sucrose	–	–
Glycerol	+	+
L-arabinose	–	–
Maltose	–	–
Cellobiose	–	–
Soluble starch	–	–
D-ribose	–	–
D-xylose	–	–
Lactose	–	–
D-melibiose	–	–
D-raffinose	–	–
D-trehalose	–	–
Propionate	–	
Acetate	+	+

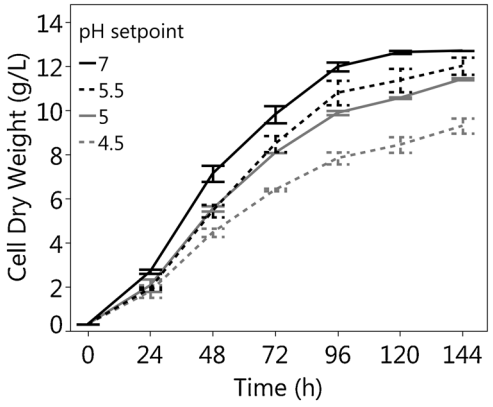

Figure 12. *Aurantiochytrium acetophilum* HS-399 tolerance to acetate toxicity at different pH setpoints. Cultures were batch-fed using an acetic acid/pH-auxostat system.

plementary Material Fig. S9). Secondary structure analysis confirmed that all sequence variations (indels) were real and not an artifact of polymerase sequencing errors (not shown).

A phylogenic tree was constructed based on an alignment that included all the *Aurantiochytrium acetophilum* HS-399 18 s rRNA sequences and probably all sequences from thraustochytrids previously used in phylogenic analyses. The resulting phylogenetic tree (https://itol.embl.de/tree/7016213025230535153559694 3#) showed that all HS-399 sequences (in blue) fell within the *Aurantiochytrium* clade. The phylogenetic analysis excluded some unaligned regions and as a consequence, the tree showed some sequences being identical. However, when the full-length sequences were examined, none of the HS-399 paralogs were identical to any of the 258 sequences (See sequences, Supplementary Material File S1). The phylogenetic tree also showed that strain HS-399 was distinct from the type species of the genus, *Aurantiochytrium limacinum* SR21.

Mitochondrial Genome

A full-length mitochondrial genome was obtained (NCBI GenBank accession number MH259702); it was 30,866 bp long, it had a 33.78% guanine-cytosine content and there was 983x coverage. Using BLAST, the HS-399 mitochondrial genome was compared to KU183024.1, a complete genome from *Schizochytrium* sp. strain TIO1101 (https://www.ncbi.nlm.nih.gov/nuccore/1041517119). A total of 56 gene features and 33 protein-coding genes were detected; BLAST analyses also showed 21 transfer RNA genes (tRNA) and two ribosomal RNA genes (rRNA) (Fig. 13, sequences of gene features Supplementary Material File S2 and annotation of gene features Supplementary Material File S3). Nucleotide sequences were evaluated and compared using Quast (Quast results in Supplementary Material File S4).

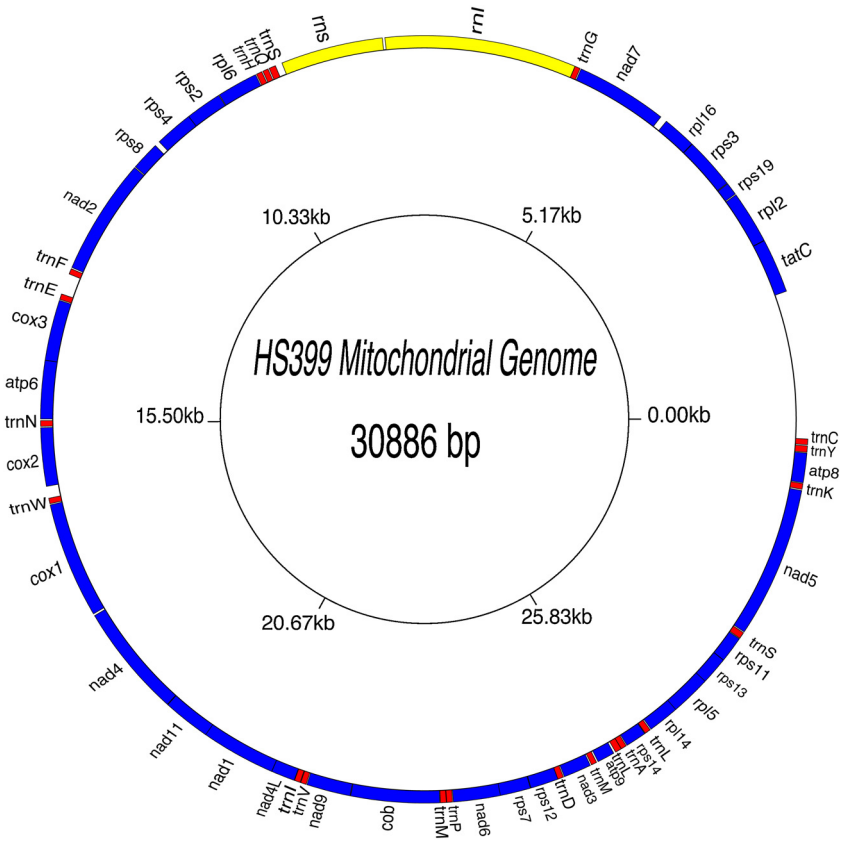

Figure 13. Gene map of the *Aurantiochytrium acetophilum* HS-399 mitochondrial genome.

F. Nuclear Genome

A clean 10,341,514 reads were assembled into 9,441 scaffolds. This Whole Genome Shotgun project has been deposited at DDBJ/ENA/GenBank under the accession QDJC00000000. The version described in this paper is version QDJC01000000.1. The genome assembly was 57,771,596 bp in total length, with an N50 equal to 16,064 bp and N75 of 7,190 bp; the guanine-cytosine content was 45% (Quast results in Supplementary Material File S5). The maximum scaffold size was 169,387 bp. There was a total of 15,131 genes de novo predicted by GeneMark-ES (genes prediction Supplementary Material File S6 and genes annotation Supplementary Material File S7) and 14,744 genes predicted by BLAST to *Aurantiochytrium limacinum* SR21 proteins sequences (Tblastn results in File S8). BUSCO (http://busco.ezlab.org), a tool that can assess genome assembly and annotation completeness with benchmarking universal single-copy orthologs, discovered 247 complete BUSCOs out of total 303 BUSCOs using eukaryote database.

The nucleotide and protein sequences comparisons between *A. acetophilum* HS-399 and *A. limacinum* strain SR21 showed 90.44% similarity at the nucleotide level (Supplementary Material File S5) and 94.62% at the protein level (Supplementary Material File S7).

Ploidy (i.e. haploid, diploid) was estimated by comparing alignments between HS-399 and SR21 (https://www.ncbi.nlm.nih.gov/genome/35766?genome_assembly_id=217282) using a simulated dataset and computing the Kolmogorow–Smirnov distances. A diploid state for vegetative cells was indicated (Supplementary Material Fig. S10).

Meiosis and Acetate Assimilation Genes

Meiosis equivalent genes were identified by first searching for meiosis gene names in NCBI to retrieve protein sequences from related organisms (e.g. *Ectocarpus*) and then by using Tblastn to search the HS-399 genome with 1e-^{6} E-value as the limiting factor. Among ten suggested core meiotic genes (dmc1, hop1, hop2, mer3, mnd1, msh4, msh5, rad51, rec8, and spo11), 12 protein sequences were retrieved; hop1 and mer3

genes each had two proteins sequences. Eight genes (9 proteins) were identified in the HS-399 genome, and they had an average of 40% similarity at the protein level. Genes *hop1* and *hop2* (3 proteins) were not found in HS-399. Next, functional protein domains, defined as "features" in NCBI database, were searched for the eight genes. The aligned regions all matched with the annotated features, suggesting that those eight genes have high potential to be functional even though the overall similarity was low. The missing genes *hop1* and *hop2* suggested that HS-399 had a unique recombination pattern during meiosis (Tblastn result in Supplementary Material File S9, meiosis protein sequences Supplementary Material File S10, and Tblastn details in Supplementary Material File S11).

Genes involved in acetate assimilation were surveyed in HS-399 draft genome. First, protein sequences were retrieved by searching GenBank for the following glyoxylate pathway genes: malate synthase MLS-glcB-aceB (P9WK16 and P42450), isocitrate liase-ICL-aceA (P42449), isocitrate lyase ICL1-icl1 (H8EVV4 and P9WKK6), and isocitrate lyase ICL2-icl2 (Q8VJU4). Next, conserved functional regions (features) which are present in these enzymes were identified. Finally, Tblastn analysis was performed for six protein sequences. All conserved functional regions were covered by HS-399 draft genome. It indicated these genes were most likely performing a similar function in acetate assimilation. The results were summarized in Supplementary Material Files S12, S13 and S14 (Tblastn result in File S12, protein sequences of acetate assimilation genes in File S13, and Tblastn details in File S14).

Discussion

A morphological comparison of *Aurantiochytrium acetophilum*, *A. limacinum* and *Schizochytrium mangrovei* Raghu-Kumar showed similarities and differences (Table 3; Honda et al. 1998; Raghu-Kumar 1988). The comparisons should be evaluated with caution because *S. mangrovei* was studied only using primarily pine pollen/seawater cultures, and the other two species were described using two different organic media. All three-species produced the Type I sporangium and zoospores; however, the number of zoospores per sporangium varied substantially, with as few as two zoospores for *S. mangrovei* and as many as 64 for *A. limacinum*. Zoospores for *S. mangrovei* were distinctly smaller ($\sim 3 \times 4$ μm) than for the other two species. Vegetative cells were also smaller for *S. mangrovei*, and those for *A. acetophilum* ranged from the smallest size to the largest size. Amoebae occurred in both *A. acetophilum* and *A. limacinum*, but no amoebae were reported for *S. mangrovei*. Amoebae were formed either directly from single cells or indirectly by amoebosporangia for *A. acetophilum*, whereas amoebae were only formed directly from single cells in *A. limacinum*. Also, amoebae from *A. limacinum* divided to produce eight zoospores whereas the amoebae of *A. acetophilum* produced one to four nonmotile vegetative cells. The size range of amoebae was also much wider for *A. acetophilum*. An amoiboid protoplasmic mass was reported for *S. mangrovei*, but this was an *Ulkenia*-type sporangium stage that was probably a result of the pine pollen culture technique (Gaertner 1977; Raghu-Kumar 1988). Finally, there were morphological features described for only a single species. Type II sporangia, cysts and sporogenous cells were reported only for *A. acetophilum*; amorphous long cells were reported only for *A. limacinum*.

Aurantiochytrium limacinum, the generitype, was based on culture strain SR21 stored in the American Type Culture Collection as strain ATCC MYA-1381. *Schizochytrium mangrovei* was based upon culture strain NIOC 90 but that strain was lost (Dr. Raghu-Kumar personal communication). Strain NIOC 90 was isolated from *Rhizophora mucronata* Lam. and *Avicennia officinalis* L. leaves collected in Goa, western India, and there was a detailed morphological description for the organism (Raghu-Kumar 1988; Table 3). The species was transferred to *Aurantiochytrium* (Yokoyama and Honda 2007) based upon gene sequences from cultures isolated from the Pacific Ocean near Hong Kong using leaves from *Kandelia candel* (L.) Druce (Fan et al. 2007); morphological data for the Hong Kong strains was not provided in either of the two papers. Furthermore, additional papers from the region do not provide morphological observations (Liu et al. 2014; Yang et al. 2010). As a consequence, we do not fully accept the transfer of *Schizochytrium mangrovei* to the genus *Aurantiochytrium* until further details are provided.

Molecular phylogenetic analyses of the 18S rRNA showed that *A. acetophilum* belongs to the *Aurantiochytrium* genus, but is genetically distinct from its type species A. *limacinum* (https://itol.embl.de/tree/7016213025230535155596943#). Further investigation into the species level phylogeny was hindered by the genetic variability of the multiple 18S rRNA paralogs of strain HS-399. Instead, we looked into the entire genome and observed a 5.38% difference with *A.*

Table 3. Morphological comparison of *Aurantiochytrium acetophilum*, *A. limacinum* and *Schizochytrium mangrovei*. Data obtained from the original taxonomic descriptions.

Species	*A. acetophilum*	*A. limacinum*	*S. mangrovei*
Strain	HS-399	SR21	NIOC-90
Character			
Vegetative cell size (μm)	5–25	7–15	6.3–9.2
Type I sporangium size (μm)	15–20	12–24	ca. 8
Zoospore size (μm)	4–6 × 4–8	5–7 × 6–8.5	2.6–3.3 × 4.1–4.8
Zoospore shape	ovoid – spherical	ovoid	ovoid
No. of zoospores/sporangium	8–32	16–64	2–32
Type II sporangium size (μm)	20–25	none	none
Amoebosporangium size (μm)	13–18	none	none
Amoeba size (μm)	4–12 × 8–35	5–8 × 12–20	none
Amoeba-produced zoospore size (μm)	none	3.5–5 × 4.5–6	none
Cyst size (μm)	25–30	none	none
Amorphous long cells	absent	present	absent
Sporogenous cells	present	absent	absent
Source of data	this paper	Honda et al. (1998)	Raghu-Kumar (1988)

limacinum (Supplementary Material Files S7 and S9), which prompt us to describe *A. acetophilum* as a new species. In view of the genetic differences, it isn't surprising that morphological differences exist between the two species (Table 3). Our studies showing a Type II sporangium, cysts and putative sexual reproduction may be found in *A. limacinum* with further study that include the special culture techniques used here. However, given the extensive video recordings in both studies, it is surprising that *A. acetophilum* amoebosporangia give rise to amoebae and that *A. limacinum* amoebae give rise to zoosporangia. At least for now, these seem to be fundamental life cycle differences between the two species.

Acetate Physiology

The growth (Fig. 10) and lipid accumulation (Table 1) of *Aurantiochytrium acetophilum* was superior to *A. limacinum*, which emphasized the industrial potential for *A. acetophilum*. The substrate assimilation study (Table 2) did not show differences among the two species, but it pointed out the capacity of *Aurantiochytrium*, as a genus, to grow on acetate as sole carbon source, which to our knowledge was not previously known for thraustochytrids. The capacity to assimilate acetate was confirmed by the identification of protein domains in HS-399 genome functionally equivalent to glyoxylate pathway genes. Acetate is an industrially relevant substrate that is cheaply produced from the petrochemical methane. The use of acetate as carbon source is typically limited by its toxicity, which increases at low pH. *A. acetophilum* showed remarkable tolerance to acetate toxicity, with marginal growth limitation observed as the pH decreased down to 5 (Fig. 12). Growth inhibition was obvious at pH 4.5, which is sufficient to kill most bacteria in pickled food (USDS Code of Federal Regulations Tile 21 Part 114.3), but *A. acetophilum* was still able to thrive. To put this in context, the culture media used to select for lactic acid bacteria are based on the use of acetate at above 5.7 (Reuter 1985). Therefore, the use of acetate as carbon source by this organism provides also an excellent opportunity for contamination control, and it was used for scale-up production using non-sterile reactors (Ganuza et al. 2018). Consequently, we chose the specific epithet *acetophilum* because of its capacity to grow on acetate.

Sexual Reproduction

Sexual reproduction is important in many ways (e.g. Speijer et al. 2015). Goodenough and Heitman (2014) state "the evolution of eukaryotic sex has featured countless prezygotic and postzygotic variations, the outcome being the segregation of panmictic populations into distinct species with distinctive adaptations." One could further refine this to state "genetic strains with distinctive adaptations", and it is for this reason that commercial companies isolate numerous strains. Searching and surveying random strains has value; however, directed sexual crossing and selection program is far more powerful. The breeding of agricultural plants and animals has been extremely successful, and it is even more impressive when one recognizes that domestication of animals and plants occurred

before recorded history. It is likely that the same revolutionary benefits of breeding will apply to today's aquaculture organisms (being domesticated in our lifetimes). Thus, in addition to academic interests in *Aurantiochytrium* sexual reproduction, there is considerable commercial interest too.

The study of sexual reproduction in Labyrinthulales and Thraustochytridiales are limited (for reviews, see Beakes et al. 2014; Porter 1990). Synaptonemal complexes were found in *Labyrinthula vitellina* spore cells, and based upon serial sections, nine complexes were counted, indicating a haploid number of nine chromosomes (Moens and Perkins 1969). The spore cells divided first by meiosis and then by mitosis, giving rise to eight zoospores (Perkins and Amon 1969). We observed fusion of two equally sized swimming cells, which suggests isogamous reproduction (Fig. 7). Our genome analysis of strain HS-399 showed the presence of eight meiosis genes, and the allele frequency distribution indicates that the vegetative cells are diploid and the life cycle is diplobiontic. The Type II sporangium (Fig. 2D–F) was found within sporogenous masses of cells, and it may be the source of gametes for *A. acetophilum*. However, there are a number of problems retarding a robust identification of meiosis and syngamy. For example, it is difficult to isolate a Type II zoosporangium without contaminating zoospores. After isolation, there are challenges when (a) following the zoosporangium by video microscopy using either an inverted microscope or a hanging drop, (b) tracking paired swimming cells, (c) documenting syngamy and zygote formation, and (d) determining the fate of the zygote. We were unsuccessful in our efforts to follow all steps continuously without interruption, but we observed numerous discrete steps that we pieced together using overlapping observations.

Eukaryotic sexual reproduction is triggered in many ways, for example, when favorable conditions (e.g. rain) help mosses reproduce or when unfavorable conditions (e.g. nutrient depletion) cause *Chlamydomonas* to reproduce. Heterogeneous environments may result in higher rates of sex (Becks and Agrawal 2010), and numerous other factors may be important (Maynard Smith 1978). Our studies found that favorable conditions (subculture into new culture medium) did not induce sexual reproduction for *A. acetophilum*. Conversely, the unfavorable condition of placing sporogenous cells into seawater or L1 medium caused at least three responses. First, some cells and sporangia produced cysts. Second, Type I zoosporangia and massive numbers of vegetative zoospores were produced. And third, Type II sporangia were produced, and these may possibly be the source of gametes. Thus, our preliminary findings suggest unfavorable environments may be a means for better understanding sexual reproduction in the Thraustochytriaceae.

Gamete fusion is a complicated process in eukaryotes, and there are several barriers that must be overcome (e.g. Hernández and Podbilewicz 2017). The steps of differentiation, tethering, adhesion, dehydration, hemifusion, pore opening and fusion were observed for *A. acetophilum* (Fig. 7) (see Hernández and Podbilewicz 2017 for description of the stages). Although we do not have a complete understanding of the sexual life cycle for *A. acetophilum*, the presence of these steps adds credence to putative sexual reproduction for this commercially valuable organism.

Overall, we have provided evidence that *A. acetophilum* is a new species. We described several life stages for the new organism, we found evidence suggesting sexual reproduction, we documented the unprecedented capacity to thrive on acetate, and we contributed complete mitochondrial and nuclear genomes for the new species. These results increase our knowledge of thraustochytrids and may lead to a better understanding of these fascinating and valuable organisms.

Methods

Organism and isolation: A field sample was collected on 13 November 2015 from the Biscayne Bay, Florida USA. The sample included a decaying red mangrove seed propagule that was streaked across an agar petri plate on 16 November 2015, and colonies were isolated from the plate on 19 November 2015 and re-streaked on agar. The agar was prepared by using the inorganic L1 medium with reduced salinity (Guillard and Hargraves 1993; salinity = 16) that was mixed 1:1 with the organically enriched *Aurantiochytrium* medium (Table S1) and solidified with 10 g/L bacto agar. An antibiotic solution was prepared using 100 mg penicillin and 25 mg streptomycin mixed in 10 ml of distilled H_2O; 100 μl of the antibiotic solution was added to 10 ml of culture (see Guillard 2005). Repeated streaking and antibiotic treatment led to axenic isolates HS-399 and HS-412 on 5 December 2015. Strain HS-399 was predominantly used for this study; strain HS-412 was only used in mating experiments. The strains were privately deposited at the Culture Collection of Algae at the University of Cologne (CCAC) and are available for research purposes upon the signature of a Material Testing Agreement.

Culture conditions: All subsequent cultures were inoculated at 1% v/v from a 24 h old culture into *Aurantiochytrium* medium (Table S1). Cells for light microscopical observation were grown in static test tubes (2–5 mL volume); cells for electron microscopy, molecular studies and physiology work were grown in 250 mL baffled Erlenmeyer flasks (100 mL volume). Flask cultures were incubated for four days in the dark using an orbital shaker (27 ± 1 °C, 170 rpm; 1-inch diameter). The

substrate concentration was adjusted to 50 g/L for the carbon assimilation and acetate flask experiments. The acetate tolerance test was carried out in a 1 L bubble column reactor (700 mL volume) aerated at 1.6 volume air per volume culture per minute. The defined medium for this test used a ¼ glutamate concentration and glycerol was replaced with 0.8 g/L sodium acetate. Cultures were maintained in the dark at 27 ± 1 °C and the residual acetate pH was controlled at each setpoint using a pH-auxostat mode with acetic acid (10% in water) as the titrant. Thus, the pH-auxostat system fed acetic acid on demand (approximately 300 mL titrant), while controlling residual acetate of the culture medium between 1.5 and 0.5 g/L throughout the fed-batch. Cell dry weight samples (10 mL) were collected daily in duplicates and vacuum filtered with glass microfiber filter papers designed to retain particles of 1.1 μm (Ahlstrom™ Grade 161). The filtrate was washed twice with 10 mL of ammonium bicarbonate 0.5 M solution and placed in an oven (105 °C) until the weight was stable.

Light microscopy: Cells were observed with a Leica DMRB light microscope equipped with DIC, phase, darkfield and brightfield optics. Photographs and videos were captured using either a Canon EOS T6i DSLR or EOS T2i DSLR camera body. Numerous observations using various culture conditions were conducted over a two-year period. High resolution images were obtained when the preparation was very thin; however, cell activity (e.g. growth, division, mating) was often impaired by the thin preparation. Therefore, low magnification wet mounts without a coverslip or hanging drop microscope slide preparations were used for these observations, although both techniques limited magnification and resolution.

Raw photographic images were transferred to Photoshop using the Canon Digital Photo Professional 4 software. Time-lapse videos were prepared from still photos taken every 10–30 sec by bringing the still images into iMovie V.4.0 (Apple Corp.). For time-lapse studies, the raw images were converted to either tiff or jpg format using Contenta Converter software (http://www.contenta-converter.com). The supplementary videos were edited using Adobe Premier Pro CC2018.

Transmission electron microscopy: Transmission electron microscopy used three fixations: Fixation 1: a cell suspension was fixed with 2% glutaraldehyde in 50 mM $NaPO_4$ pH 7.5 with 0.1 M sucrose buffer (final concentrations) for 15 min at room temperature and then for 3 h on ice. The cells were pelleted, encased with 0.9% agarose and washed four times in the same buffer over a 1 h period. Cells were post-fixed for 2 h at room temperature in 1% osmium tetroxide in buffer. The cells were washed twice with distilled H_2O and stored at 4 °C overnight. The cells were stained for 1 h at room temperature with 1% aqueous uranyl acetate, washed three times with distilled H_2O, and then dehydrated in an acetone series using 20% increments. There were four changes of 100% anhydrous acetone before infiltration with Spurr's resin and embedded in Spurr's for 24 h at 60 °C. Fixation 2: the procedure was the same as fixation 1 but with a 50 mM Na cacodylate buffer at pH 7.2 and with an ethanol dehydration series (20, 50, 75, 95%) that ended with anhydrous ethanol and propylene oxide. Infiltration and embedding were the same as Fixation 1. Fixation 3: cells were pre-fixed for 10 min with 0.5% osmium tetroxide and 2.5% glutaraldehyde in 0.1 M Na cacodylate pH 7.2 and 0.12 M sucrose. Cells were pelleted, fixed on ice for 2 h with 2.5% glutaraldehyde in 0.1 M Na cacodylate pH 7.2 and 0.12 M sucrose. Post-fixation, dehydration, infiltration and embedding were as with Fixation 2. Ultramicrotomy of thin (70 nm) sections were cut using a Leica Ultracut-R microtome and sections were collected on formvar-coated copper slot grids. Sections were stained for 7 min with 10 g/L uranyl acetate in a 50% v/v solution of ethanol and water, and then stained for 4 min with Sato's lead citrate solution. Transmission electron microscopy images were obtained using Philips CM-12 operated at 80 kV and equipped with Gatan model 791 CCD camera.

Lipid analyses and carbon assimilation experiments: Lipid analyses were carried out using the AOAC method 996.06 from centrifuged (3000 *g*, 10 °C) and freeze-dried biomass. Fatty acid methyl esters (FAME) were prepared according to the method described by Rodríguez-Ruiz et al. (1998) with nonadecanoic acid as internal standard. FAMEs were separated by GC with He as a carrier gas using BPX70 25 m × 0.22 mm i.d. column (SGE). The initial temperature of the column 205 °C was maintained for 6 min, then raised to 250 °C at a rate of 6 °C/min and maintained for another 10 min at 250 °C for a total run time of 23.5 min. The injection port and flame- ionization detector were maintained at 250 and 260 °C, respectively. Fatty acids were identified by comparison to external standards. Astaxanthin and canthaxanthin were analyzed following the Roche Index n° 2264 official method. Beta-carotene was analyzed according to EN (European Standard) method 12823 version 2:2000. Lutein and zeaxanthin were analyzed according to Royal DSM method ver. 1.5 2009.

Molecular phylogenetic analysis: Molecular phylogenetic analyses using 18S rRNA sequence comparison were initiated by growing cells of strain HS-399 on the defined medium and harvesting cells on Day 3. The flasks were dominated by lipid accumulating vegetative cells. DNA extraction was performed using a Quick-DNA TM Fungal/Bacterial Miniprep kit (Zymo Research, Irvine USA) following the directions on the manufacturer kit. The 18S rRNA gene was amplified by PCR with primers Euk1AF (CTGGTTGATCCTGCCAG) and 1520R (CTGCAGGTTCACCTAC). The ~1800 bp PCR product was separated by agarose gel electrophoresis, purified using the QIAquick® Gel Extraction Kit (Qiagen), and sequenced with the same primers. The PCR product sequences had short reads of about 200 bp before abruptly degrading, suggesting multiple 18S alleles being amplified. To obtain single reads, approximately 40 ng of the PCR product was cloned using the Zero Blunt® TOPO PCR cloning kit (ThermoFisher/Invitrogen) for 1 h at room temperature and transformed into DH5a competent *Escherichia coli* cells (New England Biolabs). Clones were sequenced using primers M13F, M13R, OTM2 (GGAGGGCAAGTCTGGTGCCAGC), and OTM4 (CCAACTAAGAACGGCCATGC) to generate distinct, full scaffolds of nearly 1800 bp. The HS-399 paralog sequences obtained after DNA cloning were compiled with all the Thraustochytriaceae sequences that we could find in the literature (Anderson et al. 2003; Bergmann et al. 2011; Bongiorni et al. 2005; Burja et al. 2006; Cavalier-Smith et al. 1994; Carmona et al. 2003; Chaplin 2015; Dellero et al. 2018; Doi and Honda 2017; FioRito et al. 2016; Fossier-Marchan 2017; Gupta et al. 2013; Hassett and Gradinger 2018; Honda et al. 1999; Hong et al. 2012; Huang et al. 2003; Kaya et al. 2011; King-Wai et al. 2009; Kumon et al. 2006; Kumon et al. 2003; Leander et al. 2004; Leipe et al. 1994; Leipe et al. 1996; Li et al. 2009; Liu et al. 2014; Maas et al. 2010; Mo et al. 2002; Moro et al. 2003; Nakazawa et al. 2014; Ragan et al. 2000; Rocke et al. 2013; Schärer et al. 2007; Stokes et al. 2002; Takao et al. 2007; Taoka et al. 2009; Tsui et al. 2009; Ueda et al. 2015; Yang et al. 2010; Yokoyama et al. 2007). *Bacillaria paxillifera* CCMP261 and *Chlorochromonas danica* were used as the outgroup.

The sequences were aligned at SSU-ALIGN (Nawrocki 2009), using a profile-based strategy, in which each target sequence is aligned independently to a covariance model that uses the 18S rRNA gene secondary structure. Poorly aligned columns were then removed from the alignment based on a

95% confidence profile. All sequences in the alignment were trimmed on Geneious version 8.0 (Kearse et al. 2012) to begin (116 bp) and end (1004 bp) at the same positions, for a total of 888 bp. Tree topology was inferred on the CIPRES high performance computing cluster (Miller et al. 2010), using the RAxML-HPC2 (Stamatakis 2014) workflow on XSEDE with the ML + thorough bootstrap (1000 bootstraps) method and the GTRGAMMA model. The resulting tree was imported into the iTOL 3 server to help visualization (Letunic and Bork 2016).

Genomic studies: Genomic DNA was eluted in 100 μL and sheared to approximately 600 bp using M220 Focused-ultrasonicator™ from Covaris (Auburn, USA). Illumina libraries were generated on the Apollo 384 liquid handler from Wafergen (Fremont, USA) using Kapa Biosystem's library preparation kit (KK8201). The DNA fragments were end-repaired and A-tailed as described in the Kapa protocol. A combined indexes and adapter (BioScientific, catalogue #520999, Austin, USA) were ligated on each individual sample so multiple samples could be multiplexed into one lane and informatically separated once the run was complete. The adapter ligated molecules were cleaned using AMPure beads (Agencourt Bioscience/Beckman Coulter, A63883), and amplified with KAPA's HIFI enzyme.

The libraries are then analyzed on an Agilent Bioanalyzer, and quantified by qPCR (KAPA Library Quantification Kit, KK4835) before multiplex pooling and sequencing a 2×300 PE flow cell on the MiSeq platform (Illumina, San Diego, USA) at the Microbiome and Genomic Core Facilities at Arizona State University (USA). The quality of raw Illumina MiSeq 2×300 bp reads was evaluated using FastQC v0.10.1, followed by adapter trimming and quality clipping by Trimmomatic 0.35. Any reads shorter than 150 bp are were eliminated. Any reads with start, end or the average quality within a 4 bp window falling below quality scores 18 were trimmed. A clean pool of 10,341,514 reads was used for assembly.

Genome assembly and annotation was carried out as follows. K-mer analysis was ran by Jellyfish 2.2.4 for genome size and heterozygosity estimation. Cleans reads were aligned to *Aurantiochytrium limacinum* SR21 ATCC MYA-1381 reference genome (http://genome.jgi.doe.gov/Aurli1/Aurli1.info.html) by BWA-MEM 0.7.13 for insert size estimation. Spades 3.7.1 with mismatch corrector mode was applied for whole-genome assembly. Full length mitochondrial contig was extracted form whole genome assembly. Both whole genome assembly and mitochondrial assembly were evaluated by comparing to the reference genome by Quast 3.2. GeneMark-ES was used for *de novo* gene prediction. Functional annotation was performed using the Trinotate pipeline, including Hmmer 3.1b2 for protein domain identification, BLAST+ for homology search, signalP v4 for signal peptide cleavage sites prediction, RNAmmer for ribosomal RNA prediction, GO (Gene Ontology) and eggNOG for orthologous group search. Additional genome annotation was performed by homology-based blastn (blast + 2.3.0) approach. GenomeVx was used for mitochondrial visualization. BUSCO ver2.0 was performed to assess genome assembly and annotation completeness with benchmarking universal single-copy orthologs. Meiosis and acetate assimilation equivalent genes were identified by first searching the gene names in NCBI to retrieve protein sequences in closest species and then Tblastn to HS-399 assembly with $1e^{-6}$ E-value.

To determine the ploidy level of HS-399 vegetative cells, the R-based package PloidyNGS (Corrêa dos Santos et al. 2017) was used to estimate ploidy from the Next Generation Sequencing data. The package plotted the allele frequency against the number of heteromorphic positions. The curve was analyzed statistically using Kolmogorov–Smirnov distance against simulated dataset provide in the package.

When searching for meiosis genes, the protein sequence sources were dmc1, rec8 and spo11 from *Emiliania huxleyi* (Lohmann) Hay & Mohler strain CCMP 1516, hop1_1 and hop1_2 from *Guillardia theta* D.R.Hill & R.Wetherbee strain CCMP 2712, hop2 and mer3_2 from *Micromonas pusilla* (R.W.Butcher) I.Manton & M.Parke strain CCMP 1545, mer3_1 from *Phaeodactylum tricornutum* Bohlin strain CCAP 1055/1, mnd1 and rad51 from *Chlamydomonas reinhardtii* P.A.Dangeard, msh4 from *Chondrus crispus* Stackh., and msh5 from *Arabidopsis thaliana* (L.) Heynh. When searching for glyoxylate pathway, the protein sequence sources were as below: malate synthase MLS-glcB-aceB (P9WK16 from *Mycobacterium tuberculosis* strain CDC 1551 and P42450 from *Corynebacterium glutamicum* ATCC 13032), isocitrate liase-ICL-aceA (P42449 from *Corynebacterium glutamicum* ATCC 13032), isocitrate lyase ICL1-icl1 (H8EVV4 from *Mycobacterium tuberculosis* ATCC 35801 and P9WKK6 from *Mycobacterium tuberculosis* CDC 1551), and isocitrate lyase ICL2-icl2 (Q8VJU4 from *Mycobacterium tuberculosis* CDC 1551).

Funding and Declaration of Interest

This work was funded by Heliae Development LLC., a private company where Eneko Ganuza and Malena Amezquita are employed and Robert A. Andersen consults. The company also contracted the services of the Arizona State Genomics and Bioinformatics Core that employs Shanshan Yang for the whole genome sequencing of the strain.

Acknowledgements

We thank Kris Scoma-Galbreath for preparing the ink drawings; David Lowry, Life Sciences Electron Microscopy Lab, Arizona State University, for TEM work; Richard Moe, University of California-Berkeley, for help with nomenclatural problems; Josh Locsin, Heliae Development, for video editing; Travis Muff, Heliae Development, and Barbara and Michael Melkonian, University of Cologne, for preliminary 18S rRNA phylogeny work; Juan Maldonado, Arizona State University Genomic Core for DNA extractions; Arizona State University Genomic Core for Illumina sequencing; Travis Muff, Heliae Development, for sequencing 18S paralogs, Mike Lamont, Heliae Development, for his support with the bioprospecting campaign; Charles E. Seller, Heliae Development, for conducting the bubble column experiment and maintaining the cultures and John and Frank Mars for their support with this project.

Appendix A. Supplementary Data

Supplementary data associated with this article can be found, in the online version, at https://doi.org/10.1016/j.protis.2019.02.004.

References

Andersen RA, Ganuza E (2018) Nomenclatural errors in the Thraustochytridiales (Heterokonta/Staminipila), especially with regard to the type species of *Schizochytrium*. Not Algar **64**:1–8

Anderson RS, Kraus BS, McGladdery SE, Reece KS, Stokes NA (2003) A thraustochytrid protist isolated from *Mercenaria mercenaria*: Molecular characterization and host defense responses. Fish Shellfish Immunol **15**:183–194

Barclay W, Weaver C, Metz J (2005) Development of a Docosahexaenoic Acid Production Technology Using *Schizochytrium*: a Historical Perspective. In Cohen Z, Ratledge C (eds) Single Cell Oils. AOCS Press, Champaign, pp 36–47

Beakes GW, Honda D, Thines M (2014) Systematics of the Straminipila: Labyrinthulomycota, Hyphochytriomycota, and Oomycota. In McLaughlin DJ, Spatafora JW (eds) The Mycota – Systematics and Evoltion Part A VII. Springer, Heidelberg, pp 39–97

Becks L, Agrawal F (2010) Higher rates of sex evolve in spatially heterogeneous environments. Nature **468**:89–92

Bergmann N, Fricke B, Schmidt MC, Tams V, Beining K, Schwitte H, Boettcher AA, Martin DL, Bockelmann AC, Reuch TBH, Rauch G (2011) A quantitative real-time polymerase chain reaction assay for the seagrass pathogen *Labyrinthula zosterae*. Mol Ecol Resour **11**:1076–1081

Bongiorni L, Jain R, Raghukumar S, Aggarwal RK (2005) *Thraustochytrium gaertnerium* sp. nov.: a new thraustochytrid stramenopilan protist from mangroves of Goa, India. Protist **156**:303–315

Burja AM, Radianingtyas H, Windust A, Barrow CJ (2006) Isolation and characterization of polyunsaturated fatty acid producing *Thraustochytrium* species: screening of strains and optimization of omega-3 production. Appl Microbiol Biotechnol **72**:1161–1169

Cavalier-Smith T, Allsopp MTEP, Chao EE (1994) Thraustochytrids are chromists, not Fungi: 18s rRNA signatures of Heterokonta. Philos Trans R Soc Lond B **346**:387–397

Carmona ML, Naganuma T, Yamaoka Y (2003) Identification by HPLC–MS of carotenoids of the *Thraustochytrium* CHN-1 strain isolated from the Seto Inland Sea. Biosci Biotechnol Biochem **67**:884–888

Chaplin MA (2015) A culture based study of non-fungal heterotrophic microbial eukaryotes from Hawaiian marine sediments. Master thesis at University of Hawaii, 125 p

Cienkowski L (1867) Über den Bau und die Entwicklichen der Labyrinthuleen. Arch f mikrosk Anat Entwicklungsmechanik **3**:274–310

Corrêa dos Santos RA, Goldman GH, Riaño-Pachón DM (2017) PloidyNGS: visually exploring ploidy with Next Generation Sequencing data. Bioinformatics **33**:2575–2576

Craze (2018) DSM, Evonik predict retailers will drive change to novel omega-3 oils in salmon industry. Undercurrentnews, https://www.undercurrentnews.com/2018/10/30/dsm-evonik-predict-retailers-will-drive-change-to-novel-omega-3-oils-in-salmon-industry/ Last accessed on 2/4/2019

Dellero Y, Cagnac O, Rose SL, Seddiki K, Cussac M, Lupette J, Cigliano RA, Sanseverino W, Kuntz M (2018) Proposal of a new thraustochytrid genus *Hondaea* gen. nov. and comparison of its lipid dynamics with the closely related pseudo-cryptic genus *Aurantiochytrium*. Algal Res **35**:125–141

Dick MW (2001) Staminipilous Fungi. Systematics of the Peronsporomycetes including accounts of the marine straminipilous protists, the plasmodiophorids and similar organisms. Kluwer Acad Publ, Boston, 670 p

Doi K, Honda D (2017) Proposal of *Monorhizochytrium globosum* gen. nov., comb. nov. (Stramenopiles, Labyrinthulomycetes) for former *Thraustochytrium globosum* based on morphological features and phylogenetic relationships. Phycol Res **65**:188–201

Fan KW, Jiang Y, Faan YW, Chen F (2007) Lipid characterization of mangrove thraustochytrid – *Schizochytrium mangrovei*. J Agric Food Chem **55**:2906–2910

FioRito R, Leander C, Leander B (2016) Characterization of three novel species of Labyrinthulomycota isolated from ochre sea stars (*Pisaster ochraceus*). Mar Biol **163**:1–10

Fossier-Marchan L (2017) A novel genus of Scottish thraustochytrids and investigation of their capacity for the production of docosahexaenoic Acid. PhD thesis at Heriot–Watt University, 168 p

Ganuza E, Izquierdo MS (2007) Lipid accumulation in *Schizochytrium* G13/2S produced in continuous culture. Appl Microbiol Biotechnol **76**:985–990

Ganuza ET, Sellers E, Sitek A, Cobos A, Hansen J, Lamont M (2018) Methods of culturing *Aurantiochytrium* using acetate as an organic carbon source. USA Patent number WO2018064036A1

Gaertner A (1977) Revision of the Thraustochytriaceae (Lower Marine Fungi) I. *Ulkenia* nov. gen., with description of three new species. Ver Inst Meeresforsch Bremerhaven **16**:139–157

Goodenough U, Heitman J (2014) Origins of sexual reproduction. Cold Spring Harb Perspect Biol **6**:1–22

Guillard RRL (2005) Purification Methods for Microalgae. In Andersen RA (ed) Algal Culturing Techniques. Elsevier, Amsterdam, pp 117–132

Guillard RRL, Hargraves PE (1993) *Stichochrysis immobilis* is a diatom, not a chrysophyte. Phycologia **32**:234–236

Gupta A, Wilkens S, Adcock JL, Puri M, Barrow CJ (2013) Pollen baiting facilitates the isolation of marine thraustochytrids with potential in omega-3 and biodiesel production. J Ind Microbiol Biotechnol **40**:1231–1240

Hassett BT, Gradinger R (2018) New species of saprobic Labyrinthulea (=Labyrinthulomycota) and the erection of a gen. nov. to resolve molecular polyphyly within the aplanochytrids. J Eukaryot Microbiol **65**:475–483

Hernández JM, Podbilewicz B (2017) The hallmarks of cell–cell fusion. Development **144**:4481–4495

Honda D, Yokochi T, Nakahara T, Erata M, Higashihara T (1998) *Schizochytrium limacinum* sp. nov., a new thraustochytrid from a mangrove area in the west Pacific Ocean. Mycol Res **104**:439–448

Honda D, Yokochi T, Nakahara T, Raghukumar S, Nakagiri A, Schaumann K, Higashihara T (1999) Molecular phylogeny of labyrinthulids and thraustochytrids based on the sequencing of 18S ribosomal RNA gene. J Eukaryot Microbiol **46**:637–647

Hong WK, Kim CH, Rairakhwada D, Kim S, Hur BK, Kondo A, Seo JW (2012) Growth of the oleaginous microalga *Aurantiochytrium* sp. KRS101 on cellulosic biomass and the production of lipids containing high levels of docosahexaenoic acid. Bioprocess Biosyst Eng **35**:129–133

Huang J, Aki T, Yokochi T, Nakahara T, Honda D, Kawamoto S, Shigeta S, Ono K, Suzuki O (2003) Grouping newly isolated docosahexaenoic acid-producing thraustochytrids based on their polyunsaturated fatty acid profiles and comparative analysis of 18S rRNA Genes. Mar Biotechnol **5**:450–457

Kaya K, Nakazawa A, Matsuura H, Honda D, Inouye I, Watanabe MM (2011) Thraustochytrid *Aurantiochytrium* sp. 18W-13a accumulates high amounts of squalene. Biosci Biotechnol Biochem **75**:2246–2248

Kearse M, Moir R, Wilson A, Stones-Havas S, Cheung M, Sturrock S, Buxton S, Cooper A, Markowitz S, Duran C, Thierer T, Ashton B, Meintjes P, Drummond A (2012) Geneious Basic: An integrated and extendable desktop software platform for the organization and analysis of sequence data. Bioinformatics **28**:1647–1649

King-Wai F, Jiang Y, Lok-Tang HO, Chen F (2009) Differentiation in fatty acid profiles of pigmented and nonpigmented *Aurantiochytrium* isolated from Hong Kong mangroves. J Agric Food Chem **57**:6334–6341

Kumon Y, Yokoyama R, Haque Z, Yokochi T, Honda D, Nakahara T (2006) A new labyrinthulid isolate that produces only docosahexaenoic acid. Mar Biotechnol **8**:170–177

Kumon Y, Yokoyama R, Yokochi T, Honda D, Nakahara T (2003) A new labyrinthulid isolate, which solely produces n-6 docosapentaenoic acid. Appl Microbiol Biotechnol **63**:22–28

Leander CA, Porter D, Leander BS (2004) Comparative morphology and molecular phylogeny of aplanochytrids (Labyrinthulomycota). Europ J Protistol **40**:317–328

Leipe DD, Tong SM, Goggin CL, Slemenda SB, Pieniazek NJ, Sogin ML (1996) 16S-like rDNA sequences from *Developayella elegans*, *Labyrinthuloides haliotidis*, and *Proteromonas lacertae* confirm that the stramenopiles are a primarily heterotrophic group. Eur J Protistol **324**:449–458

Leipe DD, Wainright PO, Gunderson JH, Porter D, Patterson DJ, Valois F, Himmerich S, Sogin ML (1994) The stramenopiles from a molecular perspective: 16S-like rRNA sequences from *Labyrinthuloides minuta* and *Cafeteria roenbergensis*. Phycologia **33**:369–377

Letunic I, Bork P (2016) Interactive tree of life (iTOL) v3: an online tool for the display and annotation of phylogenetic and other trees. Nucleic Acids Res **44**:242–245

Li Q, Chen GQ, Fan KW, Lu FUP, Aki T, Jiang Y (2009) Screening and characterization of squalene-producing thraustochytrids from Hong Kong mangroves. J Agric Food Chem **57**:4267–4272

Liu Y, Singh P, Sun Y, Luan S, Wang G (2014) Culturable diversity and biochemical features of thraustochytrids from coastal waters of Southern China. Appl Microbiol Biotechnol **98**:3241–3255

Maas MJ, Kleinschuster PAY, Dykstra SJ, Smolowitz R, Parent J (2010) Molecular characterization of QPX (Quahog parasite unknown), a pathogen of *Mercenaria mercenaria*. J Shellfish Res **9**:257–312

Marchan LF, Chang KJ, Nichols PD, Mitchell WJ, Polglase JL, Gutierrez T (2017) Taxonomy, ecology and biotechnological applications of thraustochytrids: a review. Biotechnol Adv **36**:26–46

Maynard Smith J (1978) The Evolution of Sex. Cambridge Univ. Press, Cambridge, 222 p

Miller MA, Pfeiffer W, Schwartz T (2010) Creating the CIPRES Science Gateway for inference of large phylogenetic trees. Gatew Comput Environ Work, 8 p

Moens PB, Perkins FO (1969) Chromosome number of a small protist: accurate determination. Science **166**:1289–1291

Mo C, Douek J, Rinkevich B (2002) Development of a PCR strategy for thraustochytrid identification based on 18S rDNA sequence. Mar Biol **140**:883–889

Moro I, Negrisolo E, Callegaro A, Andreoli A (2003) *Aplanochytrium stocchinoi*: a new Labyrinthulomycota from the Southern Ocean (Ross Sea, Antarctica). Protist **154**:331–340

Nakazawa A, Kokubun Y, Matsuura H, Yonezawa N, Kose R, Yoshida M, Tanabe Y, Kusuda E, Van-Thang D, Ueda M, Honda D, Mahakhant A, Kaya K, Watanabe MM (2014) TLC screening of thraustochytrid strains for squalene production. J Appl Phycol **26**:29–41

Nakazawa A, Matsuura H, Kose R, Kato S, Honda D, Inouye I, Watanabe MM (2012) Optimization of culture conditions of the thraustochytrid *Aurantiochytrium* sp. strain 18W-13a for squalene production. Bioresour Technol **109**:287–291

Nawrocki EP (2009) Structural RNA Homology Search and Alignment Using Covariance Models. PhD Thesis at Washington University, 281 p

Pan J, del Campo J, Keeling PJ (2017) Reference tree and environmental sequence diversity of Labyrinthulomycetes. J Eukaryot Microbiol **64**:88–96

Perkins FO, Amon JP (1969) Zoosporulation in *Labyrinthula* sp. : an electron microscopy study. J Protozool **16**:235–257

Porter D (1990) Phylum Labyrinthulomycota. In Margulis L, Corliss JO, Melkonian M, Chapman DJ (eds) Handbook of Protoctista. Jones and Bartlett Publ, Boston, pp 388–398

Raghu-Kumar S (1988) *Schizochytrium mangrovei* sp. nov., a thraustochytrid from mangroves in India. Trans Br Mycol Soc **90**:627–631

Ragan MA, MacCallum GS, Murphy CA, Cannone JJ, Gutell RR, McGladdery SE (2000) Protistan parasite QPX of hard-shell clam *Mercenaria mercenaria* is a member of Labyrinthulomycota. Dis Aquat Org **42**:185–190

Ratledge C (2013) Microbial oils: an introductory overview of current status and future prospects. OCL Oilseeds Fats Crops Lipids **20**:1–7

Reuter G (1985) Elective and selective media for lactic acid bacteria. Int J Food Microbiol **2**:55–68

Rodríguez-Ruiz J, Belarbi EH, Sanchez JLG, Alonso DL (1998) Rapid simultaneous lipid extraction and transesterification for fatty acid analyses. Biotechnol Tech **12**:689–691

Rocke E, Jing H, Liu H (2013) Phylogenetic composition and distribution of picoeukaryotes in the hypoxic northwestern coast of the Gulf of Mexico. Microbiol Open **2**:130–143

Schärer L, Knoflach D, Vizoso BD, Rieger G, Peintner U (2007) Thraustochytrids as novel parasitic protists of marine free-living flatworms: *Thraustochytrium caudivorum* sp. nov. parasitizes *Macrostomum lignano*. Mar Biol **152**:1095–1104

Sparrow FK (1936) Biological observations on marine fungi from the Woods Hole waters. Bull Mar Biol Lab, Woods Hole **70**:236–363

Sparrow FK (1960) Aquatic Phycomycetes. 2nd edn Univ. Mich. Press, Ann Arbor, 1187 p

Sparrow FK (1976) The Present Status of Classification in Biflagellate Fungi. In Jones EBG (ed) Recent Advances in Aquatic Mycology. Paul Elek, London, pp 213–222

Speijer D, Lukeš J, Eliáš M (2015) Sex is a ubiquitous, ancient, and inherent attribute of eukaryotic life. Proc Natl Acad Sci USA **112**:8827–8834

Stamatakis A (2014) RAxML version 8: a tool for phylogenetic analysis and post-analysis of large phylogenies. Bioinformatics **30**:1312–1313

Stokes NA, Ragone-Calvo LM, Reece KS, Burreson EM (2002) Molecular diagnostics, field validation, and phylogenetic analysis of Quahog Parasite Unknown (QPX), a pathogen of the hard clam Mercenaria mercenaria. Dis Aquat Org **52**:233–247

Takao Y, Nagasaki K, Honda D (2007) Squashed ball-like dsDNA virus infecting a marine fungoid protist *Sicyoidochytrium minutum* (Thraustochytriaceae, Labyrinthulomycetes). Aquat Microb Ecol **49**:101–108

Taoka Y, Nagano N, Okita Y, Izumida H, Sugimoto S, Hayashi M (2009) Extracellular enzymes produced by marine eukaryotes, thraustochytrids. Biosci Biotechnol Biochem **73**:180–182

Tsui CKM, Marshall W, Yokoyama R, Honda D, Lippmeier JC, Craven KD, Peterson PD, Berbee ML (2009) Labyrinthulomycetes phylogeny and its implications for the evolutionary loss of chloroplasts and gain of ectoplasmic gliding. Mol Phylogenet Evol **50**:129–140

Ueda M, Nomura Y, Doi K, Nakajima M, Honda D (2015) Seasonal dynamics of culturable thraustochytrids (Labyrinthulomycetes, Stramenopiles) in estuarine and coastal waters. Aquat Microb Ecol **74**:187–204

Yang HL, Lu CK, Chen SF, Chen YM, Chen YM (2010) Isolation and characterization of Taiwanese heterotrophic microalgae: screening of strains for docosahexaenoic acid (DHA) production. Mar Biotechnol **12**:173–185

Yokoyama R, Honda D (2007) Taxonomic rearrangement of the genus *Schizochytrium sensu lato* based on morphology, chemotaxonomic characteristics, and 18S rRNA gene phylogeny (Thraustochytridaceae, Labyrinthulomycetes): emendation of *Schizochytrium* and erection of *Aurantiochytrium* and *Oblongichytrium* gen. nov. Mycoscience **48**:199–211

Yokoyama R, Salleh B, Honda D (2007) Taxonomic rearrangement of the genus *Ulkenia* sensu lato based on morphology, chemotaxonomical characteristics, and 18S rRNA gene phylogeny (Thraustochytriaceae, Labyrinthulomycetes): emendation of *Ulkenia* and erection of *Botryochytrium*, *Parietichytrium*, and *Sicyoidochytrium* gen. nov. Mycoscience **48**:329–341